# Genome-wide chromatin interaction profiling reveals a vital role of super-enhancers and rearrangements in host enhancer contacts during BmNPV infection

Shudi Zhao, Yuedong Li, Guanping Chen, et al.

*Genome Res.* 2023 33: 1958-1974 originally published online October 23, 2023
Access the most recent version at doi:10.1101/gr.277931.123



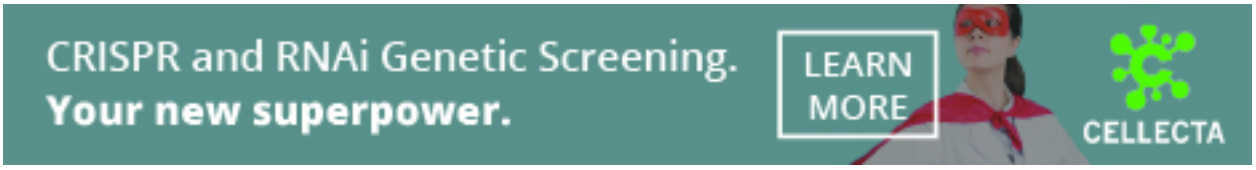

Research

# Genome-wide chromatin interaction profiling reveals a vital role of super-enhancers and rearrangements in host enhancer contacts during BmNPV infection

Shudi Zhao,[1,2] Yuedong Li,[1,2] Guanping Chen,[1,2] Xingyang Wang,[1,2] Nan Chen,[1,2] and Xiaofeng Wu[1,2]

[1]*College of Animal Sciences, Zhejiang University, Hangzhou 310058, China;* [2]*Key Laboratory of Silkworm and Bee Resource Utilization and Innovation of Zhejiang Province, Hangzhou 310058, China*

**As influential regulatory elements in the genome, enhancers control gene expression under specific cellular conditions, and such connections are dynamic under different conditions. However, because of the lack of a genome-wide enhancer–gene connection map, the roles and regulatory pattern of enhancers were poorly investigated in insects, and the dynamic changes of enhancer contacts and functions under different conditions remain elusive. Here, combining Hi-C, ATAC-seq, and H3K27ac ChIP-seq data, we generate the genome-wide enhancer–gene map of silkworm and identify super-enhancers with a role in regulating the expression of vital genes related to cell state maintenance through a sophisticated interaction network. Additionally, a radical attenuation of chromatin interactions is found after infection of *Bombyx mori* nucleopolyhedrovirus (BmNPV), the main pathogen of silkworm, which directly rearranges the enhancer contacts. Such a rearrangement disturbs the intrinsic enhancer–gene connections in several antiviral genes, resulting in reduced expression of these genes, which accelerates viral infection. Overall, our results reveal the regulatory role of super-enhancers and shed new light on the mechanisms and dynamic changes of the genome-wide enhancer regulatory network.**

**[Supplemental material is available for this article.]**

Transcriptional regulation plays a vital role in the dynamic utilization of the complex genome during development, homeostasis maintenance, and responses to external stimuli or pathogen infection (Chen and Rajewsky 2007; Spitz and Furlong 2012; Andersson et al. 2014; Roadmap Epigenomics Consortium et al. 2015; Daman and Josefowicz 2021), in which the coordination between gene promoters and enhancers is required to ensure the cell type–specific and condition-specific gene expression (Beagrie and Pombo 2016; Haberle and Stark 2018). Enhancers are noncoding *cis*-acting elements typically 200–2000 bp in length and are present upstream of or downstream from certain genes to drive their spatiotemporal expression (Shlyueva et al. 2014). Generally, they possess numerous recognition sites for sequence-specific transcription factors (TFs), by which the complexes of TFs are bound to enhancers and subsequently recruit cofactors with a variety of biochemical functions (Long et al. 2016; Furlong and Levine 2018; Andersson and Sandelin 2020). Through these various TFs and cofactors with activating or repressive activities, enhancers exert their overall regulatory function in controlling transcription from target core promoters irrespective of their orientation and distance (Smale and Kadonaga 2003; Visel et al. 2009; Schoenfelder and Fraser 2019; Field and Adelman 2020). Super-enhancers (SEs) are clusters of enhancers with high chromatin accessibility and densely enriched interacting factors, which have greater activation capacity than most of the typical-enhancers (TEs) and can regulate genes with especially important roles in cell identity and fundamental biological processes (Hnisz et al. 2013; Whyte et al. 2013). Because the positions of enhancers relative to the target core promoters can be arbitrary, making out the correspondence between enhancers and their target genes becomes a challenge, although it is of great significance to clarify these regulatory relationships and reveal their biological functions for further investigation.

The regulatory activity of enhancers and the correspondence with certain promoters are closely related to the chromatin accessibility, histone modification, and DNA interaction frequency (The ENCODE Project Consortium 2012; Shibata et al. 2012; Whalen et al. 2016). In eukaryotic cells, the genome is dynamic and nonrandomly organized in the nucleus. Therefore, the chromatin epigenomic signatures and three-dimensional (3D) architecture are dynamically remodeled during different processes or under different conditions, such as embryonic development (Li et al. 2018; Li et al. 2019), cell differentiation (Vidaurre and Chen 2021), aging (Sun et al. 2018; Braga et al. 2020), carcinogenesis (Dawson and Kouzarides 2012; Jia et al. 2017), abiotic stress (Chang et al. 2020b), and pathogen infection (Zhang and Cao 2019; Liang et al. 2022). Consequently, the interaction regulatory network between enhancers and their target genes varies under diverse circumstances, making it possible to adjust the expression of genes with specific functions spatially and temporally to adapt to the changing status.

DNA viruses are nucleic acid–based obligate intracellular pathogens, which commonly replicate and assemble in the host nucleus (Weitzman and Fradet-Turcotte 2018). In the process of infection, a number of DNA viruses dominate chromatin epigenetic markers

**Corresponding author: wuxiaofeng@zju.edu.cn**
Article published online before print. Article, supplemental material, and publication date are at https://www.genome.org/cgi/doi/10.1101/gr.277931.123.




33:1958–1974 Published by Cold Spring Harbor Laboratory Press; ISSN 1088-9051/23; www.genome.org

and restructure the host genome 3D architecture, thus reprogramming gene expression and modulating the infection status, including hepatitis B virus (HBV) (Yang et al. 2020), adenovirus type 5 (Ad5) (Moreau et al. 2018), influenza A (IAV) (Heinz et al. 2018), Epstein–Barr virus (EBV) (Moquin et al. 2018; Kim et al. 2020; Wang et al. 2020), human papillomavirus (HPV) (Cao et al. 2020; Groves et al. 2021), and baculovirus (Laakkonen et al. 2008; Shoji et al. 2021). Such extensive and conserved changes contribute to converting the host intranuclear environment to a suitable circumstance for efficient viral replication and transcription. However, how these alterations of chromatin state affect gene expression and infection progression remains poorly explored. Therefore, it is fundamental and necessary to investigate the dynamic changes in the enhancer regulatory network caused by chromatin reconstruction during infection and its downstream impact on viral invasion.

Baculoviruses are a large group of invertebrate-specific DNA viruses with rod-shaped nucleocapsids (Rohrmann 2013). Because of their high virulence and rapid establishment of infection, baculoviruses have been widely used for biological pest control and heterologous protein expression (Lacey et al. 2015; Mishra 2020). As a representative member of baculoviruses, *Bombyx mori* nucleopolyhedrovirus (BmNPV) is the main pathogen of the silkworm, an important economic insect for silk production (Kondo and Maeda 1991; Gomi et al. 1999), and causes great economic losses to the sericulture all over the world (Jiang and Xia 2014). During baculovirus infection, viral DNA is synthesized in the virogenic stroma (VS), and the host chromatin is marginalized as a result of VS expansion (Nagamine et al. 2008), implying that chromatin state is changed during infection. We have illustrated in our previous study that BmNPV infection remodeled the accessibility of host chromatin and altered the organization of host chromatin in epigenomic regulation accompanied by a global alteration in host gene expression (Kong et al. 2020). However, how these changes affect the gene expression regulatory networks remains elusive, and little is known about the enhancer regulatory landscape because genome-wide chromatin interaction information is lacking.

Long-range interactions between specific pairs of loci can be evaluated with 3C (Dekker et al. 2002), 4C (Simonis et al. 2006; Zhao et al. 2006), and 5C (Dostie et al. 2006); however, these methods require a set of target loci and are incapable of unbiased genome-wide analysis. As a derivative of the above-mentioned techniques, Hi-C is a high-throughput method developed for genome-wide analysis of chromosomal conformation, in which biotin labeling is used to allow library construction, and all the contact relationships are preserved to generate high-throughput data that indicate the contact frequency (Lieberman-Aiden et al. 2009). Therefore, Hi-C can be used to conduct unbiased genome-wide chromatin 3D conformation analysis and establish the all-to-all DNA interaction landscape.

In this study, Hi-C, epigenetic, and transcriptomic data were combined with biochemical assays to build the global and accurate genome-wide enhancer map in the silkworm for investigation of the enhancer functions and to elaborate the dynamic changes in the host enhancer regulatory network during baculovirus infection.

## Results

### Epigenomic state and DNA interaction participate in regulating gene expression

In eukaryotes, open chromatin regions and histone modifications are not uniformly distributed across the genome. Of them, the former represent active genomic elements, and the latter are frequently enriched at distinct genomic locations, where their presence is correlated either positively or negatively with transcriptional activity (Millán-Zambrano et al. 2022). In general, active enhancers are marked with both H3K4me1 and H3K27ac (Heintzman et al. 2009), whereas H3K4me2, H3K4me3, and H3K9ac are correlated with transcriptionally active genes (Santos-Rosa et al. 2002; Morillon et al. 2005; Tserel et al. 2010). Oppositely, H3K9me2, H3K9me3, and H3K27me3 are responsible for transcriptional silencing (Tserel et al. 2010; Padeken et al. 2022).

To testify the roles of these epigenomic signatures in regulating the transcriptional activity, ATAC-seq and H3K27ac ChIP-seq data obtained in our previous study, together with ChIP-seq data of several other histone modifications obtained from public databases, were reanalyzed to generate the epigenomic landscape in a silkworm cell line (BmN). As revealed in the circle diagram, the distribution trends of accessible chromatin regions and activating histone modifications all over the genome were consistent with those of RNA polymerase II (RNA Pol II) (Fig. 1A; Supplemental Fig. S1A). Furthermore, the accumulation of these epigenomic features around each transcription start site (TSS) was visualized and quantified, which revealed that accessible regions and activating modifications were centralized at the TSS, whereas the repressive histone modifications were scattered around the TSS with no obvious peak (Fig. 1B). Notably, chromatin accessibility and H3K27ac accumulation presented a high level in the upstream regions of TSS (Fig. 1B), implying their extra functions other than regulating the promoter activity.

Furthermore, previous studies have indicated that the interaction between *cis*-acting elements and promoters is required for transcriptional regulation (Beagrie and Pombo 2016; Schoenfelder and Fraser 2019). Therefore, it is surmised that DNA interaction frequently appears in the regulatory elements. To confirm this hypothesis, Hi-C analysis was conducted to investigate the 3D chromatin structures of BmN cells (Fig. 1C). The chromatin interaction profiles were highly correlated between the two replicate samples of each group (Supplemental Fig. S1B–D), indicating high reproducibility and reliability of the Hi-C data in assessing chromatin interaction. According to our Hi-C profiling results, the DNA interaction frequency diminished progressively as the distance to the TSS increased (Fig. 1D). To further characterize the genomic functional elements in the interaction regions, the genomic features were assessed. As a result, >30% of the interaction regions were predominantly overlapped with promoter elements, which only accounted for 2.75% of the whole genome (Fig. 1E), indicating that DNA interaction was nonrandom and the promoter regions were more favored. Taken together, these results showed that the epigenomic state and chromatin interaction played important roles in transcriptional regulation.

### Construction of the genome-wide map of enhancer–gene connections

To explore how chromatin state affected gene expression, the activity-by-contact (ABC) model reported previously was used to construct the genome-wide map of enhancer–gene connections across the silkworm genome (Fulco et al. 2019). Because the interaction frequency decays as their genomic distance increases (Supplemental Fig. S10A,B), to ensure both the precision and recall of enhancer identification, only genes and chromatin-accessible elements within 5 Mb were considered. After the ABC scores were calculated, altogether 17,776 enhancer–gene connections

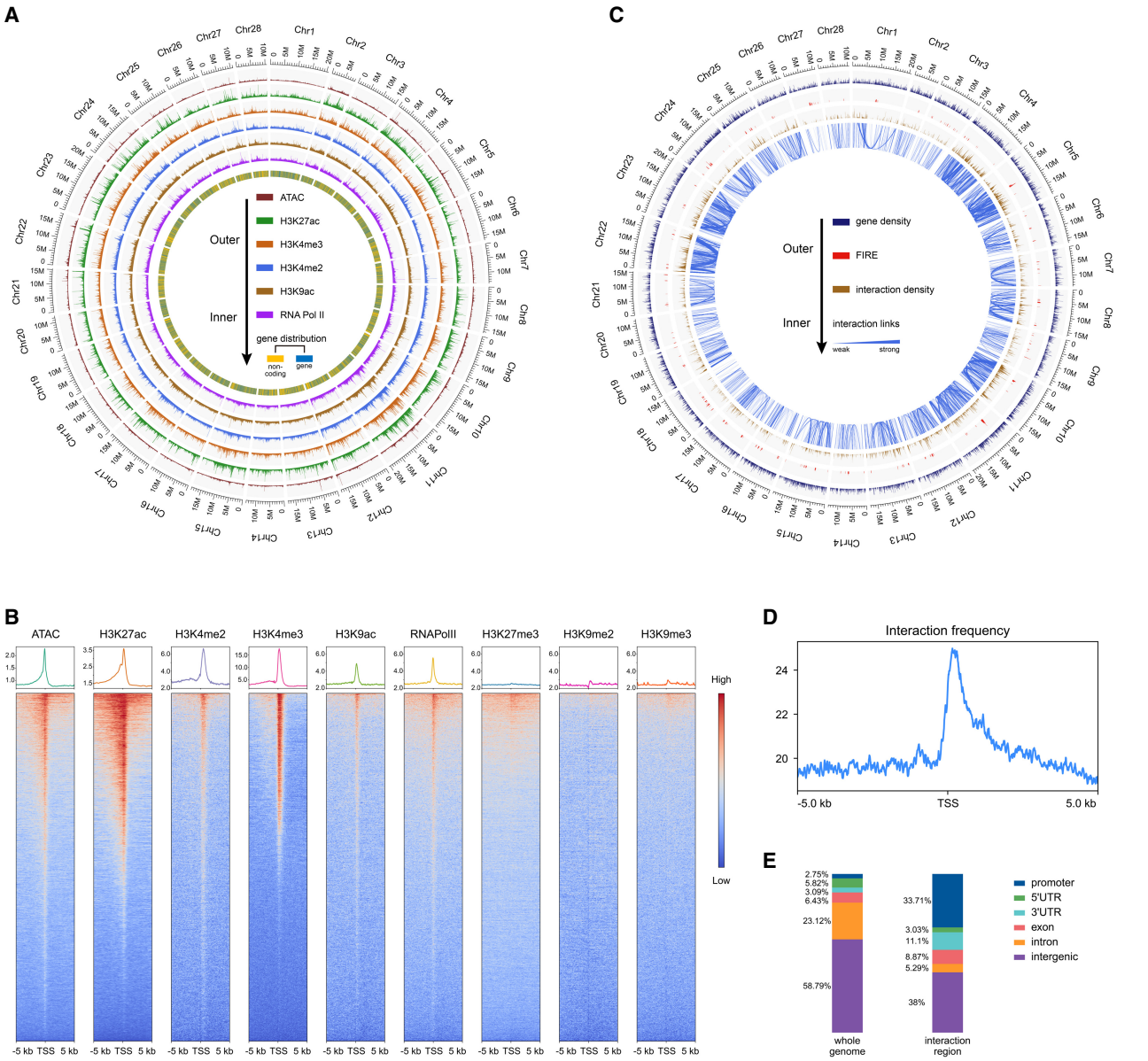


**Figure 1.** Epigenomic signatures and chromatin interactions are tightly related to transcriptional regulation. (*A*) Landscape of chromatin accessibility and histone modifications in the silkworm genome. (*B*) Enrichment of chromatin accessibility and histone modifications around all the 16,880 transcription start sites (TSSs) in the silkworm genome. (*C*) Landscape of significant *cis*-interactions in the genome. (FIRE) Frequently interacting regions. (*D*) Average interaction frequency around all the 16,880 TSSs. (*E*) Enrichment of the significant interacting regions on indicated genomic features, including the promoter, 5′ untranslated region (5′ UTR), 3′ untranslated region (3′ UTR), exon, intron, and intergenic region.

were identified for 7199 individual genes and 7269 unique enhancers, comprising 7.79 Mb of the enhancer sequence. On average, each enhancer was predicted to regulate 2.4 genes, whereas each gene was predicted to be regulated by 2.5 enhancers (Fig. 2A; Supplemental Table S2).

In the predicted enhancer regions, much higher accessibility and more evident enrichment of activating enhancer marks were found than those in the peripheral regions, including an extra enhancer signature that was not involved in this model (Fig. 2B). To further validate these predictions, the transcriptional activities of enhancer-associated genes were examined, and it was discovered that these genes were generally expressed at higher levels than others (Fig. 2C); such a result was also found in various tissues of different silkworm strains (Supplemental Fig. S12). Together, these statistical data suggested that the generated enhancer map was of high reliability and that the enhancer–gene connections contributed significantly to transcriptional activation.

## SEs drive the high-level expression of their target genes

In mammalian cells, the flanking interval and epigenomic states are reported to be different between enhancers. The clustered and long-spanned enhancers contain extremely high levels of activating marks and are thereby called super-enhancers (Whyte et al. 2013). Such characteristics were also observed from our results (Fig. 2A). To determine whether SEs existed in the silkworm

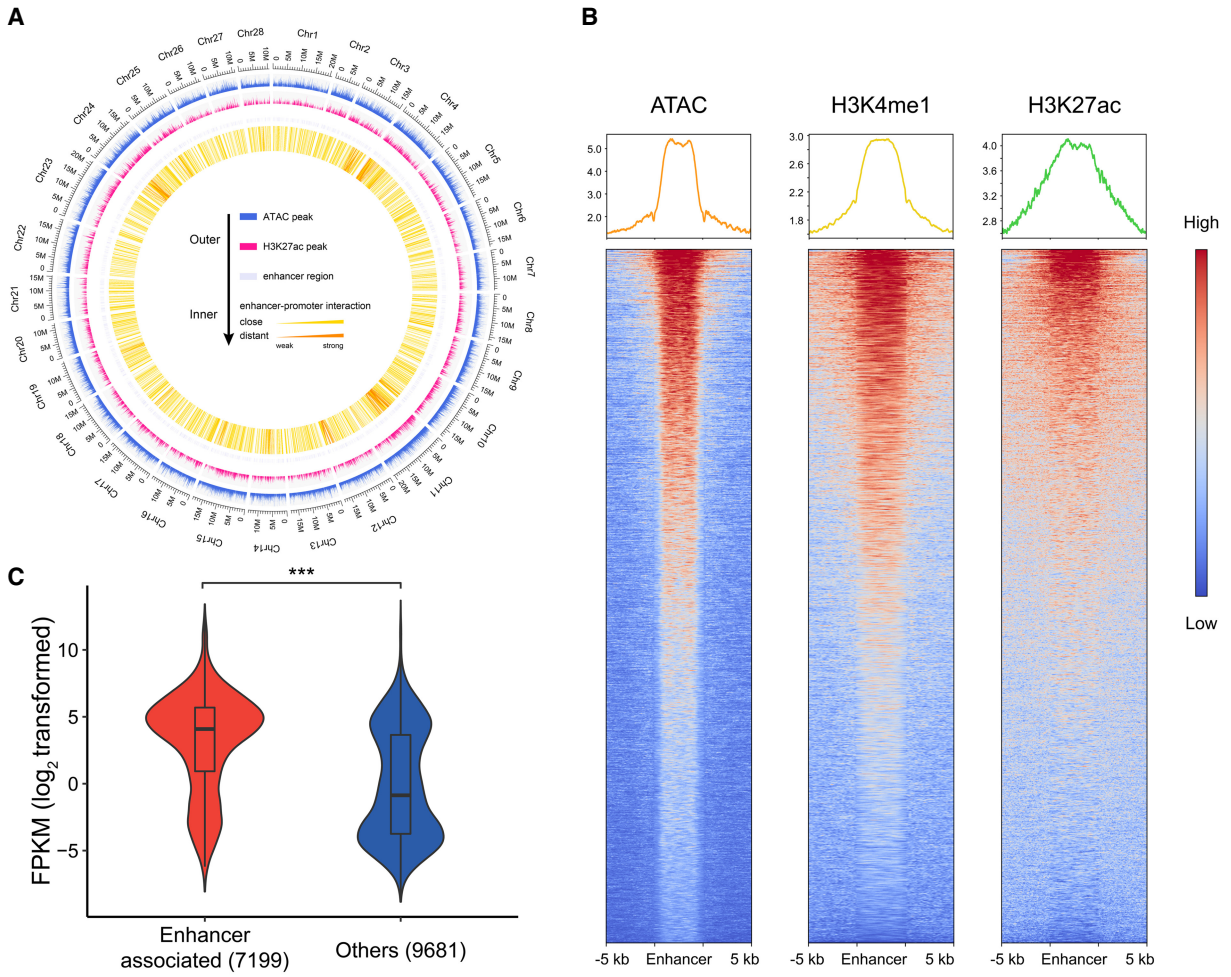


**Figure 2.** Construction of the genome-wide enhancer map. (*A*) Landscape of enhancer–promoter contacts and the peak distribution of chromatin accessibility and H3K27ac in the genome. (*B*) Enrichment of chromatin accessibility and enhancer marks around all the 7269 enhancer regions. (C) Relative expression level of enhancer-associated genes and nonassociated genes (log-transformed data). Boxes represents lower quartile, median, and upper quartile; whiskers denote the fifth and 95th percentiles. Violin plots denote the density estimates. Two-tailed Wilcoxon rank-sum test: (***) $P<10^{-15}$.

genome, the ROSE algorithm was used (Whyte et al. 2013), which stitched enhancers existing within 12.5 kb of each other and ranked them according to the H3K27ac signal (Fig. 3A). Based on the results of ROSE, 70 SEs consisting of 467 single enhancers were identified (Fig. 3A; Supplemental Fig. S2C; Supplemental Table S3). The rank of normalized chromatin accessibility and H3K4me1 signal were also visualized. As observed, H3K27ac had the sharpest transition, which was therefore considered as optimal (Supplemental Fig. S2A). The identified SEs had significantly higher levels of H3K4me1, H3K27ac, and accessibility, together with much more peaks of these activating signatures than those in TEs (Fig. 3B,C; Supplemental Fig. S2B).

To further identify the roles of these SEs in transcriptional regulation, enhancers were assigned to their target genes in line with the generated enhancer map. There were 220 genes found to be associated with the 70 identified SEs (Supplemental Table S4), and their expression levels were analyzed statistically using RNA-seq data. As expected, the SE-associated genes showed higher transcription levels than those of genes associated with TEs (Fig. 3D; Supplemental Fig. S2D).

The small molecule JQ1 has been shown to specifically inhibit SEs and has minimal effects on TEs (Lovén et al. 2013). BRD4 is a vital factor in SE-induced transcriptionally activation and is the target of JQ1 (Wang et al. 2019). To verify the role of JQ1 in the silkworm, BmN cells were transfected with pIZ-BmBRD4-HA for transient expression of HA-tagged BmBRD4, which was verified via western blot and immunofluorescence (Supplemental Fig. S3B,C). Afterward, ChIP-seq was conducted on BmBRD4. As a result, the occupation of BmBRD4 on the identified SEs decreased significantly after JQ1 treatment (Fig. 3E,F), whereas the occupation on TEs showed no obvious decline (Fig. 3F), indicating that the BRD4 binding at SEs was more sensitive to JQ1 treatment than at TEs. Furthermore, to testify the transcriptional regulation activity of SEs, RNA-seq was also conducted in JQ1-treated cells. It was found that only SE-associated genes were down-regulated significantly after JQ1 treatment instead of TE-associated genes (Fig. 3G).

In summary, these results indicated that SEs conferred stronger regulatory activities than TEs.

## SEs play vital roles in cell state maintenance

To further identify the functional properties of SEs, the functions of SE-regulated genes were annotated based on Gene Ontology

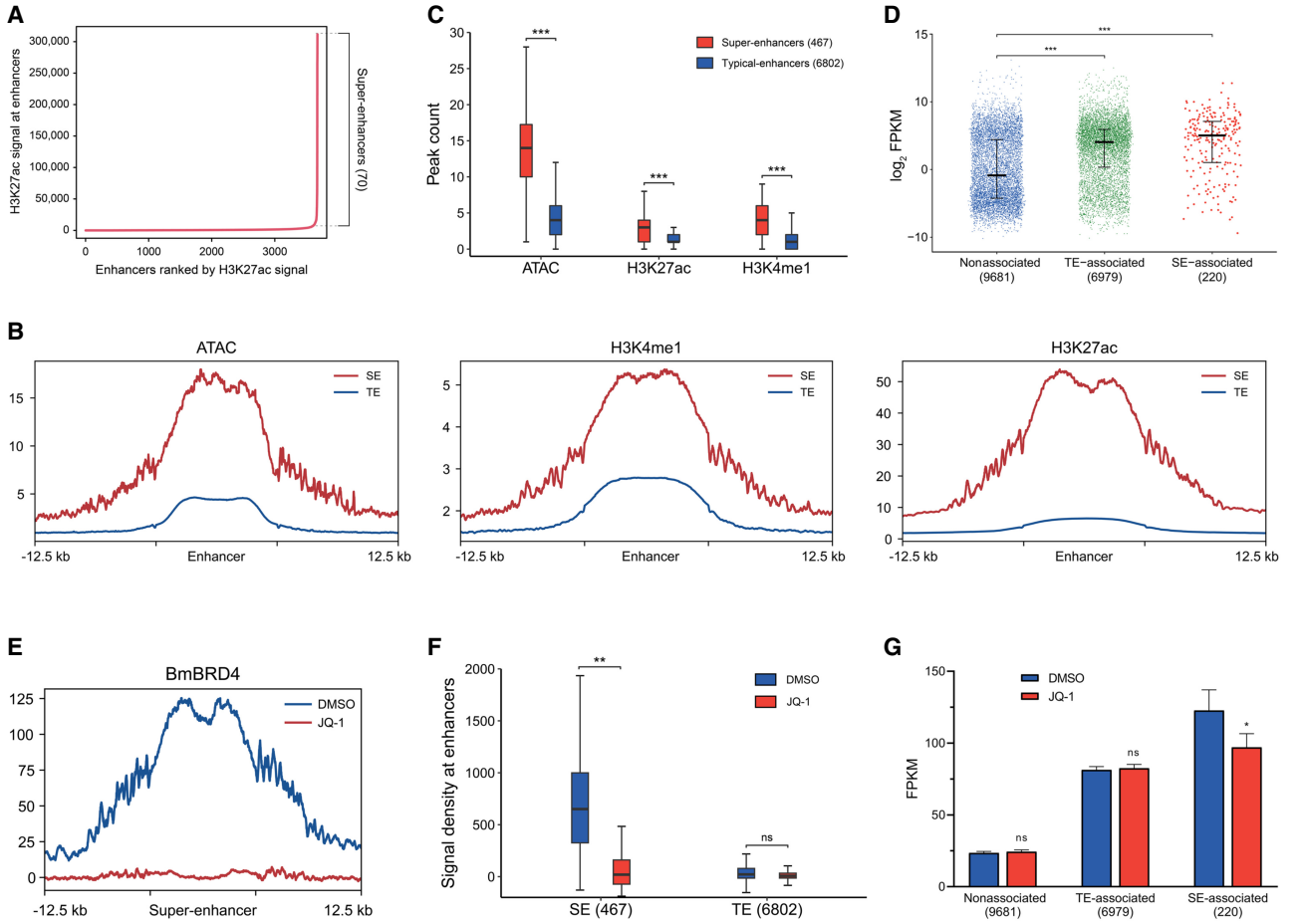


**Figure 3.** Identification and characterization of super-enhancers (SEs). (*A*) Distribution of H3K27ac ChIP-seq signal across the enhancers. H3K27ac occupancy is not evenly distributed across the enhancer regions, with a subset of enhancers (70 SEs) containing exceptionally high amounts of H3K27ac signal. (*B*) Enrichment of chromatin accessibility and enhancer marks around the identified SEs (red) and typical-enhancers (TEs; blue). (*C*) Peak count of chromatin accessibility and enhancer marks at the identified SEs (red) and TEs (blue). Box plots indicated the median (*center* of box), lower and upper quartiles (bounds of box), and minimum and maximum values (bars). Two-tailed Wilcoxon rank-sum test: (***) $P<10^{-15}$ versus TEs. (*D*) FPKM of all the nonassociated, TE-associated, and SE-associated genes. The plotted data of each gene were represented by the average FPKM of the gene calculated from the RNA-seq results of three independent libraries. Error bar indicates the median (*center* of bar) and lower and upper quartiles (bars). Two-tailed Wilcoxon rank-sum test: (***) $P<10^{-15}$ versus nonassociated genes. (*E*) Enrichment of BmBRD4 around the identified SEs in DMSO-treated (blue) or 0.5 μM JQ1-treated (red) cells. DMSO treatment was served as the control. (*F*) Signal density of BmBRD4 ChIP-seq at the identified SEs and TEs in DMSO-treated (blue) or 0.5 μM JQ1-treated (red) cells. DMSO treatment was served as the control. Box plots indicated the median (*center* of box), lower and upper quartiles (bounds of box), and minimum and maximum values (bars). Two-tailed *t*-test: (**) $P=0.003418$ versus the control. (*G*) FPKM of all the nonassociated, TE-associated, and SE-associated genes in DMSO-treated or 0.5 μM JQ1-treated cells. DMSO treatment was served as the control. The plotted data of each gene were represented by the average FPKM of the gene calculated from the RNA-seq results in three independent libraries. Error bar indicates the SE. Paired *t*-test: (*) $P=0.04245$ versus the control.

(GO) and Kyoto Encyclopedia Genes and Genomes (KEGG) analyses (Supplemental Fig. S2E,F). As shown in the KEGG classifications, SEs were preferentially associated with genes implicated in protein metabolism, from synthesis to degradation, and cell survival (Supplemental Fig. S2E). The enriched GO terms presented more detailed pathways correlated with SEs (Supplemental Fig. S2F), consistent with the KEGG results that SEs were essential in the vital biological processes. Among the enriched clusters, four sets of genes attracted our attention. The first one was *ATPase*, a key member in oxidative phosphorylation for the maintenance of energy supplement (Junge and Nelson 2015), which was regulated by a distant SE (Fig. 4A). The second set included *Actin-3* and *Actin-4*, which were two clustered genes responsible for transport and cell morphology maintenance (Dominguez and Holmes 2011) and were associated with one SE and three TEs (Fig. 4B). The third one was *IAP*, an inhibitor of apoptosis (Hamajima et al. 2016), which was correlated with one SE and three distant TEs (Fig. 4C). The last set included *HSP*s, the molecule chaperones for protein folding and the resistance of heat shock (Richter et al. 2010), which were simultaneously regulated by a long-spanned SE (Fig. 4D). In addition, all these genes were expressed at relatively high levels among the SE-associated genes (Supplemental Table S4).

To validate the importance of the SE-induced regulatory activity in the silkworm, BmN cells were treated with JQ1. After 48 h of treatment, apoptosis was clearly observed in JQ1-treated cells (Supplemental Fig. S3E). Moreover, according to flow cytometric analysis, the apoptosis rate increased in a dose-dependent manner (Fig. 4E). In addition, cell viability decreased with the increase of JQ1 concentration (Fig. 4F). The mRNA levels of these selected genes in JQ1-treated cells were further examined. It was found

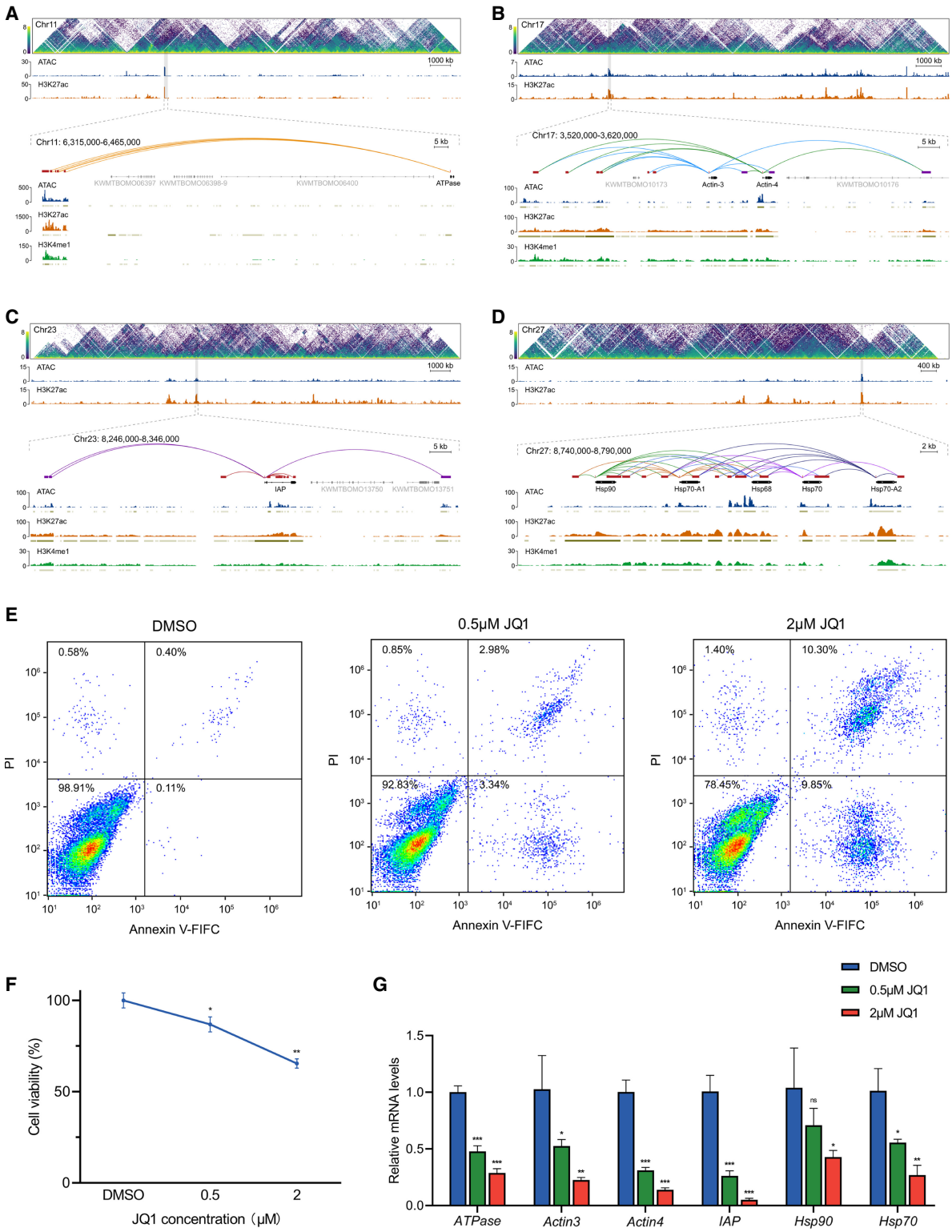


**Figure 4.** Roles of SEs in cell state maintenance. (*A–D*) Profiles of DNA interaction and normalized epigenetic signatures depicting the regulatory network of SEs at *ATPase* (*A*), *Actin* (*B*), *IAP* (*C*), and *HSP* (*D*) loci. (*E*) Flow cytometric assay for cell apoptosis detection in JQ1-treated cells. The DMSO treated cells were used as the control. Cells were distinguished as viable (Annexin V-FITC−/PI−), early apoptotic (Annexin V-FITC+/PI−), late apoptotic (Annexin V-FITC +/PI+), and necrotic (Annexin V-FITC−/PI+). (*F*) Cell viability of JQ1-treated cells. Three biological replicates per treatment were analyzed (n = 3). DMSO treatment was served as the control. Error bar indicates the SD. Two-tailed *t*-test: (*) $P = 0.01764$, (**) $P = 0.003305$ versus the control. (*G*) qRT-PCR analysis for the expression of SE-associated genes in JQ1-treated cells. *Rpl32* was used as the reference gene for data normalization. Three technical replicates for each of the three biological replicates per treatment were analyzed (n = 3). DMSO treatment was served as the control. Error bar indicates the SD. Two-tailed *t*-test: (*) $P < 0.05$, (**) $P < 0.01$, (***) $P < 0.001$ versus the control.

that the expression of these SE-associated genes decreased with the increase of JQ1 concentration (Fig. 4G), whereas the expression of two TE-associated control genes showed no significant change (Supplemental Fig. S3D). Collectively, these results showed that SEs robustly activated the expression of genes involved in vital biological processes to maintain cell state.

### BmNPV infection rearranges the enhancer regulatory network by changing the chromatin state

It is a widespread phenomenon that DNA viruses manipulate host chromatin organization (Lieberman 2008). We have reported in our previous study that BmNPV infection resulted in an substantial increase of chromatin accessibility, whereas such an increase showed no positive, but even negative, correlation with gene expression (Kong et al. 2020), which is anomalous because open chromatin regions are conducive for active gene expression. Therefore, the density of the active enhancer mark H3K27ac across the genome and that around the accessible peaks were examined. According to our observation, the overall H3K27ac levels in mock- and BmNPV-infected cells were consistent even though the global distribution of H3K27ac was detected to be more steady with several conspicuous peaks disappearing in BmNPV-infected cells (Supplemental Fig. S5A,B). However, the modification level in open chromatin regions and the correlation between the two epigenetic signatures dropped after 48 h of infection (Fig. 5A; Supplemental Fig. S6A), showing that BmNPV mediated the desynchronization between chromatin accessibility and H3K27ac modification, which might result in a loss of transcriptional regulatory activity of the accessible regions after viral infection.

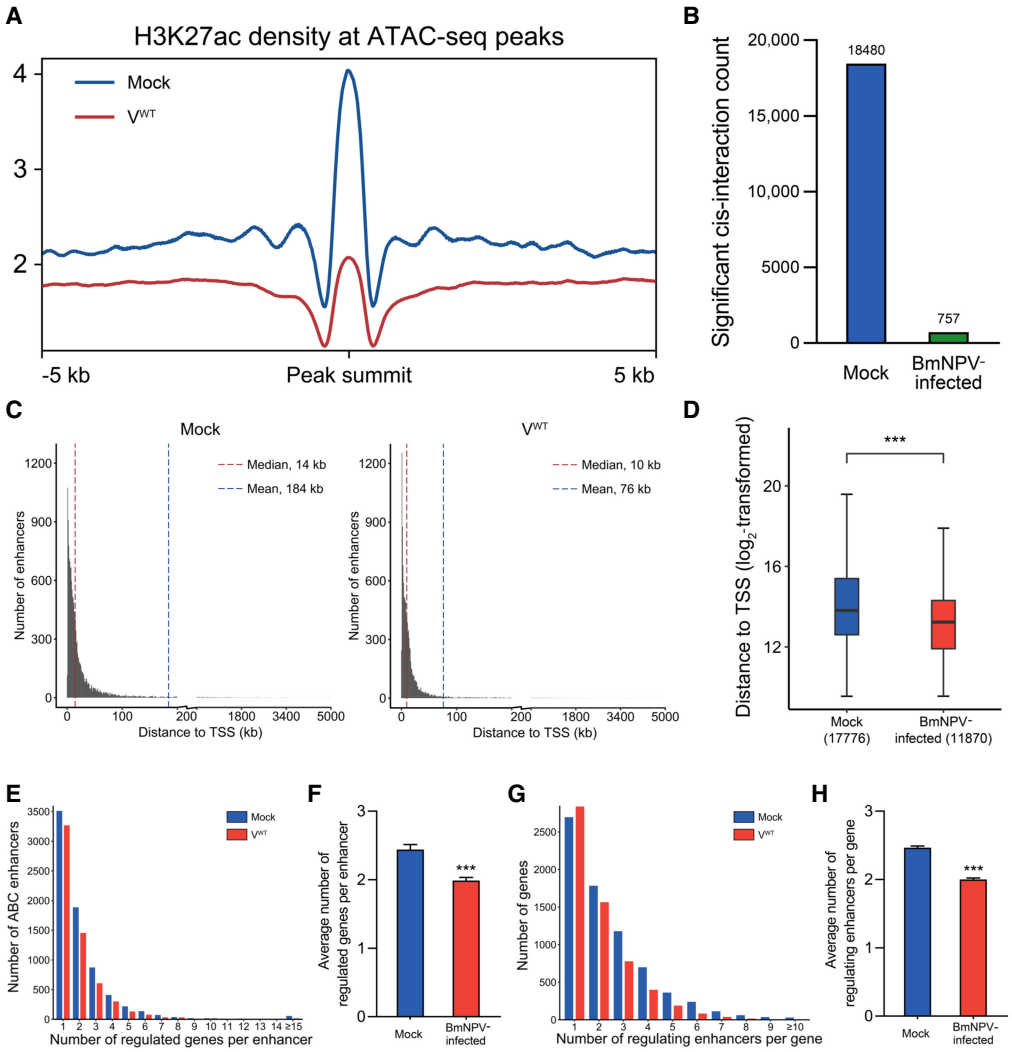


**Figure 5.** BmNPV remodels enhancer contacts by desynchronizing chromatin accessibility with H3K27ac modification and weakened *cis*-interaction. (*A*) Changes of the H3K27ac density at the ATAC-seq peaks after BmNPV infection. (*B*) BmNPV infection drastically attenuates *cis*-interaction. (*C*) Distances from all the predicted enhancers to the TSS of their target genes in mock- and BmNPV-infected cells. (*D*) Box plots of the distances showed in *C*. The median (*center* of box), lower and upper quartiles (bounds of box), and minimum and maximum values (bars) were indicated. Two-tailed *Wilcoxon* rank-sum test: (***) $P<10^{-15}$ versus mock. (*E*) Distribution histogram of the number of genes regulated by enhancer. All the identified enhancers (7269 in mock-infected cells and 5957 in BmNPV-infected cells) were analyzed. (*F*) Average number of genes regulated by enhancer plotted in *E*. Error bar indicates the SE. Two-tailed *t*-test: (***) $P<10^{-8}$ versus mock. (*G*) Distribution histogram of the number of regulating enhancers per gene in mock- and BmNPV-infected cells. All the enhancer-associated genes (7199 in mock-infected cells and 5920 in BmNPV-infected cells) were analyzed. (*H*) Average number of regulating enhancers per gene plotted in *G*. Error bar indicates the SE. Two-tailed *t*-test: (***) $P<10^{-15}$ versus mock.

The chromatin interaction landscape in BmNPV-infected cells was also explored by Hi-C assay, with an aim to investigate the BmNPV-induced effect on host genome 3D architecture. After 48 h of infection, the chromatin interaction frequency declined radically and globally (Supplemental Fig. S6B), and the number of significant interactions also decreased sharply (Fig. 5B). Cell viability was monitored after infection and no obvious infection-induced cell death at 48 h post infection (p.i.) (Supplemental Fig. S4A,B), indicating that the decrease of chromatin interaction was mediated by BmNPV infection instead of viability loss. To determine whether these changes of chromatin state altered the enhancer contacts, the enhancer–gene map of BmN cells was constructed at 48 h p.i. based on the combination of ATAC-seq, H3K27ac ChIP-seq, and Hi-C data, as described above (Supplemental Table S5). Although there were new enhancer–gene contacts assembled after BmNPV infection (Supplemental Fig. S6D–F), statistical analysis revealed that the infection reduced the number of enhancer–promoter pairs (Supplemental Fig. S6C). In particular, it especially affected the distant connections (Fig. 5C,D). In addition, fewer genes were regulated by each enhancer, and each gene was correlated with less enhancers on average after viral infection (Fig. 5E–H). It was also found that the ratio of SE–gene contacts disturbed by viral infection was significantly higher compared with TE–gene contacts (Supplemental Fig. S11A,B). To sum up, based on the above findings, BmNPV infection disturbed the intrinsic enhancer–promoter regulatory relationships and weakened the regulatory capacity of enhancer–promoter network by two ways, namely, desynchronizing the accessibility with H3K27ac modification and repressing host chromatin interaction.

## The rearrangement of enhancer contacts impedes the activation of antiviral genes in response to BmNPV infection

It is known that the alternation of enhancer contacts is directly related to the transcriptional regulation of genes originally associated with enhancers. Therefore, we first annotated the functions of these genes by GO and KEGG analyses (Fig. 6A,B). According to the KEGG analysis results, the terms related to immune system and information processing in viruses were mostly enriched (Fig. 6A), indicating that genes regulated by the intrinsic enhancer contacts participated in the resistance of viral infection. Additionally, the GO term related to nucleosome assembly was concurrently enriched (Fig. 6B). Meanwhile, gene set enrichment analysis (GSEA) results showed that genes in this cluster were significantly and holistically down-regulated (Fig. 6C), hinting that the expression of these genes in the enriched term was affected by the changed enhancer contacts, which might be the underlying mechanism of the nucleosome depletion and increased chromatin accessibility during BmNPV infection.

To further investigate the impact of the remodeled enhancer regulatory network on cellular antiviral immunity, we examined the transcription levels of BmNPV-resistant genes reported previously (Chang et al. 2020a). At 48 h p.i., most of the non-enhancer-associated genes were up-regulated (Fig. 6E,F), reflecting the antiviral immunity in response to BmNPV infection. However, although a small part of enhancer-associated antiviral genes was expressed at higher levels after infection, which might be regulated by other mechanisms, the majority of enhancer-associated antiviral genes failed to be activated (Fig. 6D,F). Therefore, it was assumed that BmNPV-induced disturbance of enhancer contacts led to transcriptional deactivation. To prove this hypothesis, eight down-regulated enhancer-associated antiviral genes were randomly selected, as annotated in the volcano plot (Supplemental Fig. S8A). In the putative enhancer regions of these genes, the chromatin accessibility did not obviously decline, whereas a substantial loss of H3K27ac modification was observed at 48 h p.i. (Fig. 7A–H), strongly supporting our hypothesis of the desynchronization between chromatin accessibility and enhancer marks. Simultaneously, the interactions between these regions and target promoters were weakened after viral infection (Fig. 7A–H).

The regulatory activities of these calculated enhancers were validated by dual luciferase reporter assay. As expected, all the cloned enhancers significantly improved the expression levels of their target genes, with the exception of two enhancers of *KWMTBOMO16000* (Fig. 7I). Also, Hi-C results of high resolution were shown to prove the interaction between these enhancers and their target promoters from the distances they work in the genomic context (Supplemental Fig. S8B), indicating high reliability of the predicted enhancer–gene connections.

Considering that the infection affected the enhancer regulatory contacts by making changes to the chromatin state, the dual luciferase reporter system should be introduced into the genome instead of into free vectors to verify the BmNPV-induced enhancer deactivation. Therefore, three affected enhancers were randomly selected and cloned into the integrated dual luciferase vector harboring *piggyBac* ITR to transpose the reporter sequence to host chromatin (Supplemental Fig. S9C), and the vectors containing the three separate promoters without their regulating enhancers served as the control (Supplemental Fig. S8C). Apparently, the transcriptional regulatory activities of these enhancers were impaired by viral infection (Fig. 7J), whereas the transcriptional activities of the separate promoters were not significantly affected (Supplemental Fig. S8D). In all, these results illustrated that the enhancer-induced activation of antiviral genes was obstructed owing to the rearrangement of the enhancer regulatory network.

## Transcriptional deactivation of antiviral genes facilitates viral infection

The transcriptional deactivation of these selected BmNPV-resistant genes during viral infection was characterized by qPCR. The results showed that all these eight genes were down-regulated significantly at 48 h p.i. (Fig. 8A; Supplemental Fig. S4C), consistent with the RNA-seq data (Supplemental Fig. S8A). Moreover, the expression of these selected genes regulated by all of their connected enhancers was markedly down-regulated after BmNPV infection compared with that of luciferase reporter genes regulated by transposed single enhancers (Figs. 7J, 8A), which could be interpreted by the fact that all the associated enhancers of a certain gene exert the joint regulatory effect.

Subsequently, to further estimate the impact of transcriptional deactivation of these genes on BmNPV infection, the eight selected genes were knocked down via dsRNAs, and the silencing efficacy was confirmed by qPCR (Fig. 8B). At 48 h post dsRNA transfection, the gene-silenced cells were infected with BmNPV, and the effect on viral infection was assessed by quantifying the viral titers and gDNA copies at various time points. As a result, infection and replication significantly accelerated at 24 h p.i. and 48 h p.i. in all of these gene-silenced samples. To be specific, the viral titers increased to 1.8- to 11.0-fold, and the gDNA levels elevated to 1.7- to 3.3-fold of the control at 48 h p.i. (Fig. 8C–J). The increase of viral titers was even spotted as early as 12 h p.i. in the absence of four genes among them (Fig. 8D, 8F, and 8H), whereas the raised gDNA levels were observed at 12 h p.i. in all the samples (Fig.

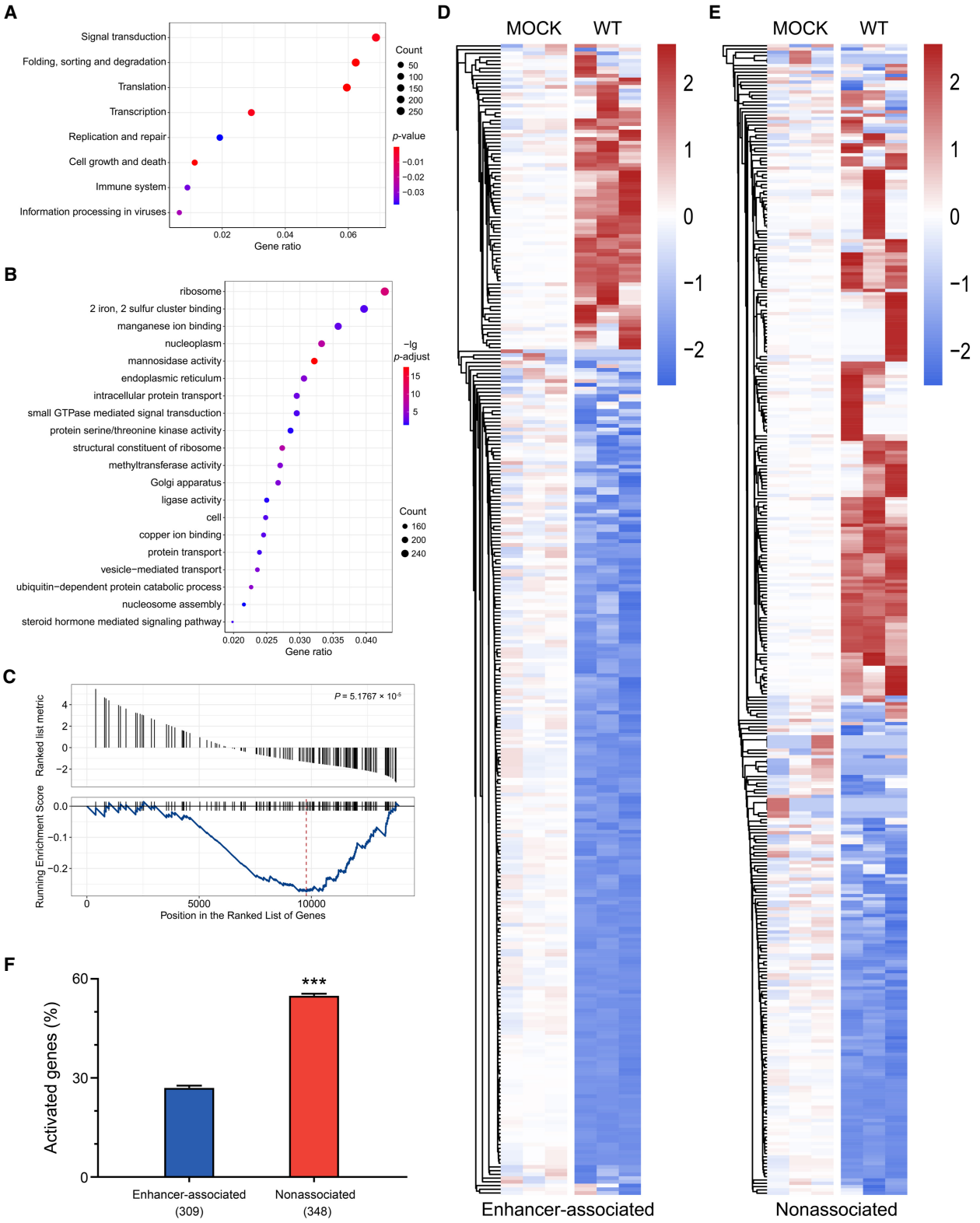


**Figure 6.** Enhancer-induced transcriptional stimulation on genes related to nucleosome assembly and BmNPV resistance is impeded after BmNPV infection. (*A*,*B*) Biological processes of KEGG terms (*A*) and GO terms (*B*) enriched in enhancer-associated genes. (*C*) Enrichment plots of the gene set related to nucleosome assembly. The GSEA result showed a significant and holistic down-regulation of the genes in this cluster. (*D*,*E*) Heatmap of the changes in enhancer-associated (*D*) and nonassociated (*E*) antiviral genes in mock- and BmNPV-infected cells at 48 h p.i. Data from three RNA-seq libraries are presented separately. Color-coding indicates $\log_2$-transformed fold changes relative to mock infection. (*F*) Percentage of transcriptionally activated genes in the two categories of antiviral genes in *D* and *E*. Two-tailed *t*-test: (***) $P<10^{-6}$.

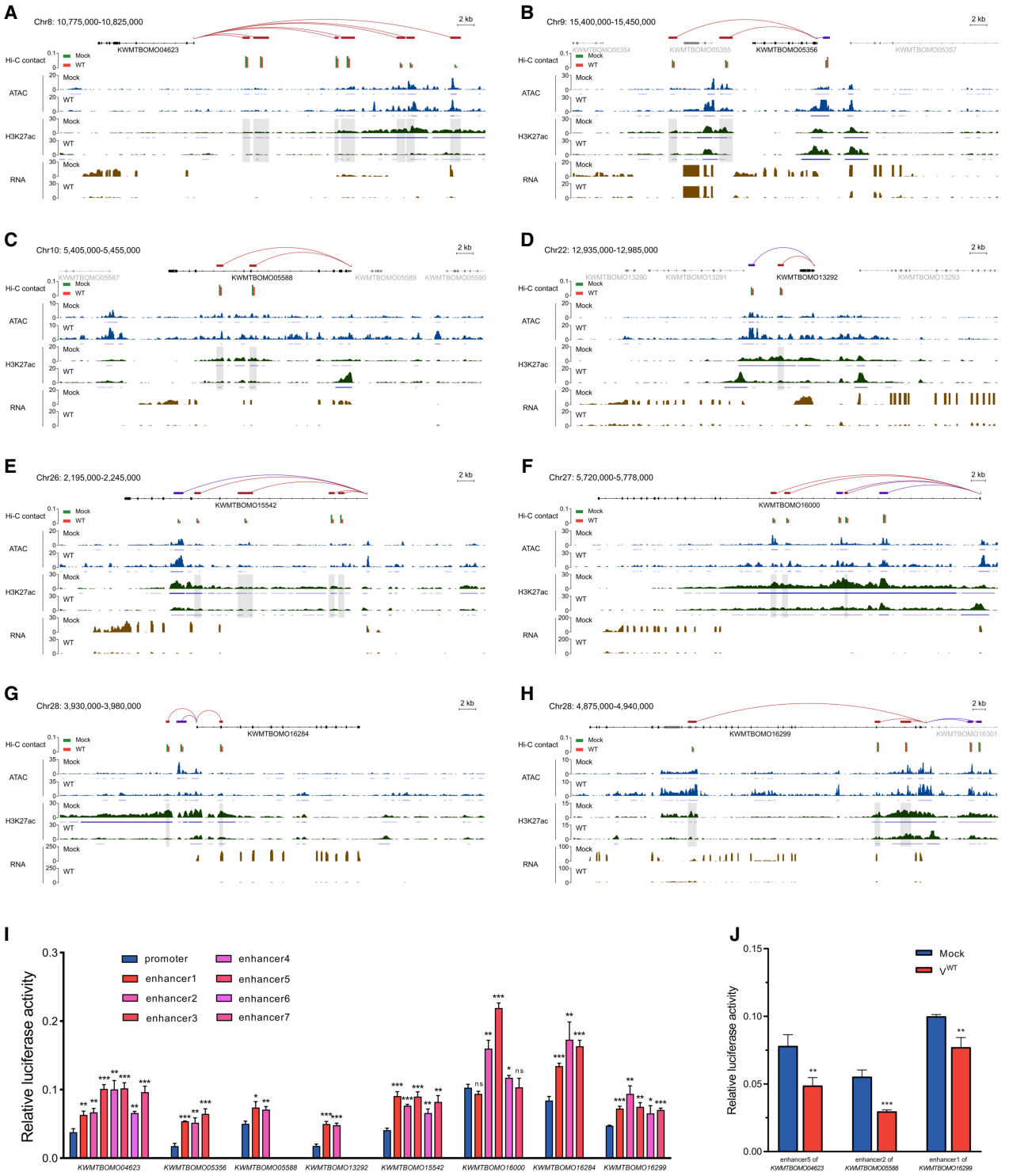


**Figure 7.** Impact of BmNPV on enhancer contacts impedes the transcriptional activation of several antiviral genes. (*A–H*) Normalized ATAC-seq, H3K27ac ChIP-seq, RNA-seq profiles, and Hi-C contacts showing the regulatory network of enhancers at eight antiviral gene—*KWMTBOMO04623* (*A*), *KWMTBOMO05356* (*B*), *KWMTBOMO05588* (*C*), *KWMTBOMO13292* (*D*), *KWMTBOMO15542* (*E*), *KWMTBOMO16000* (*F*), *KWMTBOMO16284* (*G*), and *KWMTBOMO16299* (*H*)—loci in uninfected cells (mock) and after 48 h of BmNPV infection (WT). Shaded regions represent decreased H3K27ac levels at the accessible enhancer regions after BmNPV infection. (*I*) Enhancer activity determined by dual luciferase reporter assay. Two technical replicates for each of the three biological replicates per treatment were analyzed (n = 3). The vector with null enhancer served as the control. Error bar indicates the SD. Two-tailed *t*-test: (*) $P < 0.05$, (**) $P < 0.01$, (***) $P < 0.001$ versus the control. (*J*) BmNPV infection impaired the activating activity of enhancers associated with antiviral genes. Two technical replicates for each of the three biological replicates per treatment were analyzed (n = 3). Error bar indicates the SD. Two-tailed *t*-test: (**) $P < 0.01$, (***) $P < 0.001$ versus mock.

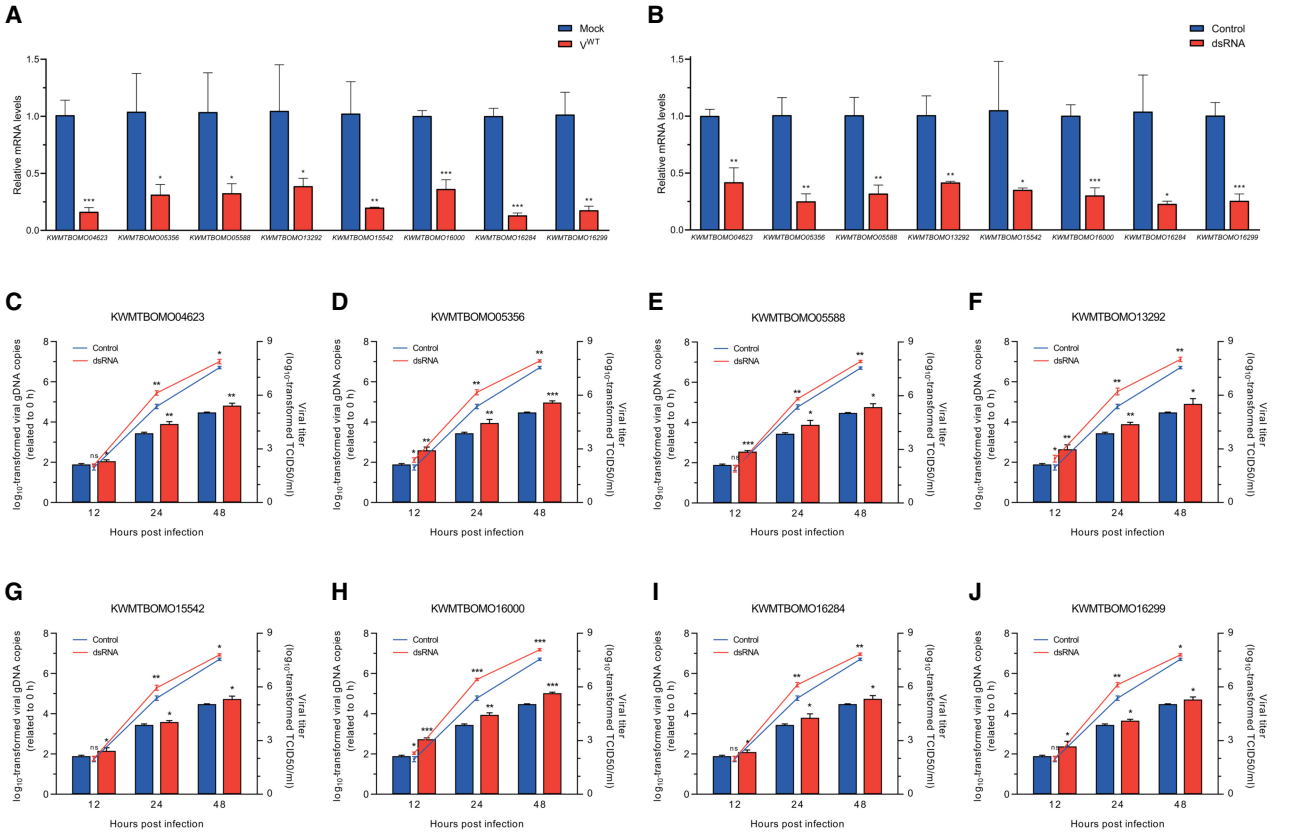


**Figure 8.** Obstruction of the transcriptional activation of antiviral genes facilitates viral infection. (*A*) qRT-PCR analysis for changes in the expression of antiviral genes at 48 h p.i. *Rpl32* was used as the reference gene for data normalization. Three technical replicates for each of the three biological replicates per treatment were analyzed (n = 3). Error bar indicates the SD. Two-tailed *t*-test: (*) $P < 0.05$, (**) $P < 0.01$, (***) $P < 0.001$ versus mock. (*B*) qRT-PCR confirmed the decline of antiviral gene expression in BmN cells treated with corresponding dsRNAs at 48 h post transfection relative to the dsCtr-transfected control group. *Rpl32* was used as the reference gene for data normalization. Three technical replicates for each of the three biological replicates per treatment were analyzed (n = 3). Error bar indicates the SD. Two-tailed *t*-test: (*) $P < 0.05$, (**) $P < 0.01$, (***) $P < 0.001$ versus the control. (*C–J*) Viral growth curves determined by $TCID_{50}$ endpoint dilution assays and replication kinetics determined by qRT-PCR analysis in cells treated with corresponding dsRNAs of the indicated antiviral gene (log-transformed data). Viral gDNA copies were determined by quantification of the DNA copies of viral gene *gp41*, which were normalized to *rpl27* and presented relative to the data at the 0-h p.i. time point. Three technical replicates for each of the three biological replicates per treatment were analyzed for viral gDNA measurements (n = 3), and three biological replicates per treatment were analyzed for titer determination (n = 3). Error bar indicates the SD. Two-tailed *t*-test: (*) $P < 0.05$, (**) $P < 0.01$, (***) $P < 0.001$ versus the control.

8C–J). Overall, these data showed that the decreased expression of BmNPV-resistant genes caused by the rearrangement of the enhancer regulatory network provided a favorable condition for speedy viral replication and spread in a relatively early stage.

## Discussion

In this study, Hi-C assay was performed to investigate the chromatin interaction in the silkworm genome, and epigenome, transcriptome, and biochemical assays were conducted in combination to comprehensively elucidate the roles and dynamic change of enhancers. As revealed from our data, SEs existed in the silkworm genome and played vital roles in cell state maintenance. During BmNPV infection, desynchronization between chromatin accessibility and enhancer marker H3K27ac took place concomitantly with chromatin interaction attenuation. Such changes of chromatin state led to the radical reorganization of the intrinsic enhancer regulatory network, which disturbed the activation of antiviral genes and therefore promoted viral infection (Fig. 9). These findings provide a novel insight into the relevance between chromatin state and genome-wide transcriptional regulation, and broaden the vision in viral domination in the host genome organization.

Because the stimulating effect of enhancers on transcription from target core promoters is independent of their orientation and distance (Visel et al. 2009; Schoenfelder and Fraser 2019), it is challenging to make out the correspondence between enhancers and their target genes. Previous effort has identified enhancers in the silkworm genome (Cheng et al. 2018), whereas the rule to define target genes of enhancers according to their distance to the nearest TSS can hardly ensure high precision and recall. To overcome the limitation, both epigenetic and Hi-C data were combined to assign enhancers to target genes by taking their contact frequency into consideration, which was more accurate and comprehensive with the capability to identify distant-acting enhancers (Figs. 2C, 4A–D, 7A–I). In addition, the enhancer–promoter map generated in this study can serve as the effective source to investigate adaptive regulation of gene expression in various status.

The significant roles of SEs have been extensively reported in mammalian cells, although relevant studies in insects are sparse and inchoate. Their existence and function have only been confirmed in *Drosophila*, in which SEs were found to be related to the

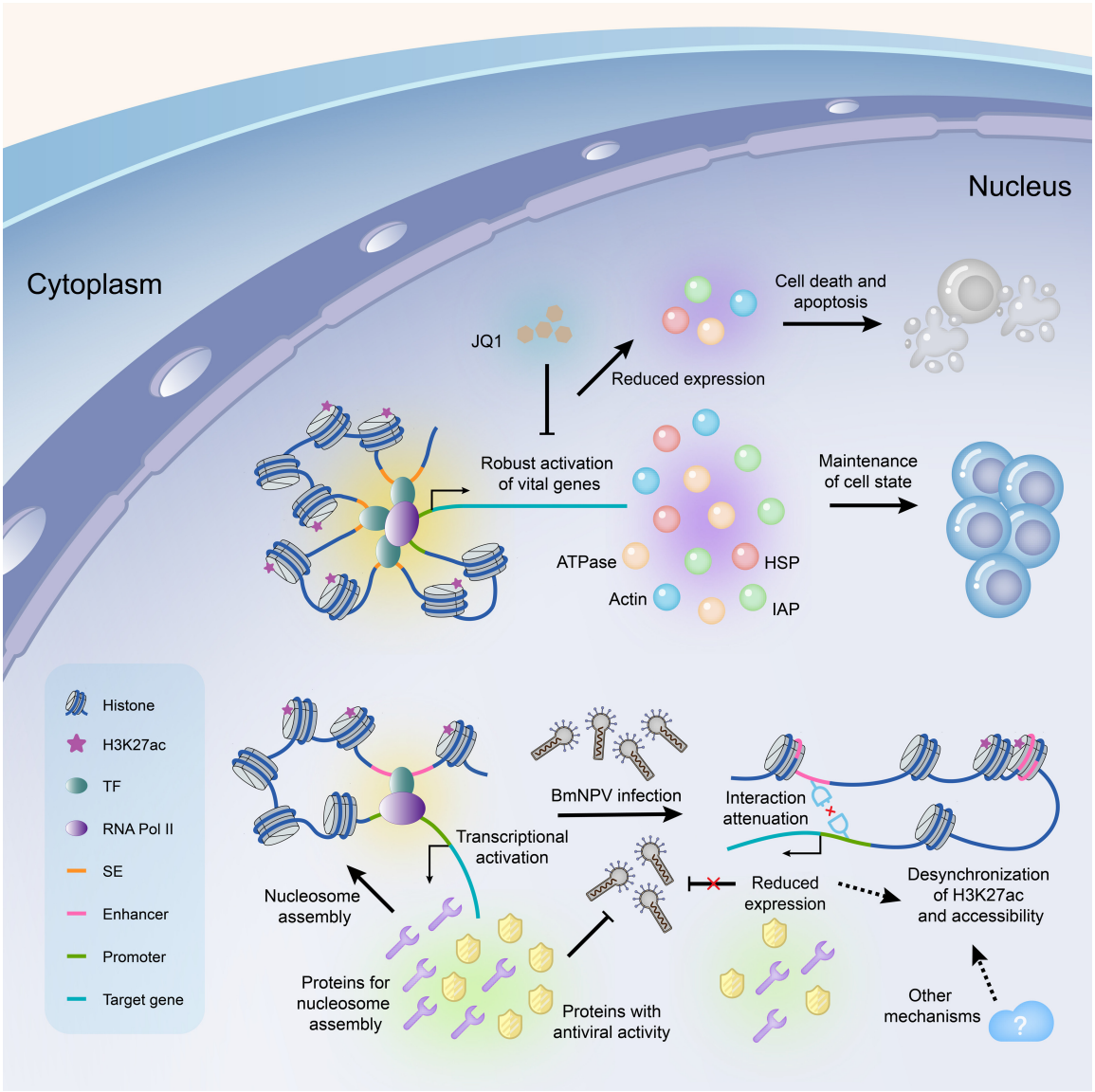


**Figure 9.** Summary of the roles of SEs and changes in enhancer regulatory network during BmNPV infection. SEs were clusters of enhancers with high chromatin accessibility and densely enriched interacting factors. In BmN cells, SEs are associated with vital genes in cell state maintenance and ensure robust activation of them. Specifically repressing the regulatory activity results in reduced expression of these vital genes and therefore leads to cell death and apoptosis. In uninfected cells, enhancers play a significant role in the activation of genes related to nucleosome assembly and BmNPV resistance. At the very late stage of BmNPV infection, accessible regions and H3K27ac distribution become staggered, causing reduced activation potential of the intrinsic enhancer regions. Additionally, viral infection radically attenuates chromatin interaction, and these two changes jointly disturb the original enhancer regulatory network, leading to inadequate expression of antiviral genes and nucleosome assembly factors. Such deregulation facilitates viral infection and may account for the increased accessibility mediated by BmNPV. This schematic is modeled on our data, and dotted lines indicate the possible underlying mechanisms based on extrapolation of data. The summary graph was generated using Adobe Illustrator CC 2018.

stage- and sex-specific gene expression in neurons, and might affect the reproductive behaviors (Palmateer et al. 2021). This study is the first to identify SEs in the silkworm and reveal their roles in vital biological processes, which expand the knowledge of SEs in insects. Nevertheless, considering the robust activating ability of SEs and the close relation between enhancer–gene contacts and the variable chromatin state in diverse conditions (Dawson and Kouzarides 2012; Jia et al. 2017; Li et al. 2018, 2019; Sun et al. 2018; Zhang and Cao 2019; Braga et al. 2020; Chang et al. 2020b; Vidaurre and Chen 2021; Liang et al. 2022), the dynamic changes of the enhancer regulatory network and the roles of SEs in insect disease, development, sex determination, and biological and abiotic stresses remain to be further investigated. In mammalian cells, the regulatory pattern of SEs is different from that of TEs (Whyte et al. 2013; Sabari et al. 2018). Our observation that JQ1 treatment suppressed the expression of SE-associated genes instead of TE-associated genes was consistent with the results obtained in mammals, which supports the surmise that the action mechanisms of SE and TE were different in insects. However, the SE-specific functional factors and how they act on the target promoters, in which phase separation and super-enhancer RNA (seRNA) may play a certain role, remain elusive (Hnisz et al. 2017; Xiao et al. 2021).

In our previous study, a broad increase of chromatin accessibility accompanied by nucleosome depletion was reported during BmNPV infection, but the changes of accessibility are not positively correlated with alternations in gene expression (Kong et al. 2020). Here, this phenomenon was interpreted by the desynchronization of epigenetic signatures. In uninfected cells, the enhancer mark–enriched regions overlapped with ATAC-seq peaks (Fig. 5A), which indicated the high accessibility in enhancers, thus ensuring the recruitment of TFs by these *cis*-elements for transcriptional regulation. After infection, the increased chromatin accessibility mediated by BmNPV was irregular and pathological. Consequently, the two requisites for *cis*-activation were staggered (Figs. 5A, 7A–H), causing the declined activating potential of the open regions. This discovery is consistent with our earlier observation that regions with gained accessibility after infection were preferentially enriched in the intergenic and intron regions, which show a lower regulatory capacity. Restriction of nucleosome assembly is a common phenomenon during viral infection, which involves functional inhibition of various host factors (Wang et al. 2008; Çevik et al. 2017; Chen et al. 2022). In this study, genes responsible for nucleosome assembly were down-regulated holistically after BmNPV infection (Fig. 6C), which might account for the increased accessibility. Nonetheless, whether it is related to the desynchronization of open regions and H3K27ac modification remains to be further explored.

Hi-C assay on BmNPV-infected cells revealed a radical attenuation of host chromatin interaction, which was the direct cause of interrupted enhancer–promoter connections (Fig. 5B; Supplemental Fig. S6B). Containment of the host chromatin interaction has also been reported for IAV (Heinz et al. 2018), although it is not the only outcome of viral infection, such as EBV infection, which forms chromatin loops to activate key oncogenes and inactivate tumor suppressor genes (Jiang et al. 2017). Anyway, improved viral infection is the consequence of almost all the virus-induced alternations of host genome 3D architecture. However, although the virus-induced changes of chromatin interaction have become commonplace, such a global attenuation of host chromatin interaction during BmNPV infection is extremely rare. Regrettably, we have little knowledge about the underlying mechanisms of BmNPV-mediated abatement of chromatin interaction, that would rearrange the enhancer–promoter interaction. Several possible causes may relate to the attenuated host chromatin interaction, such as the competitive inhibition caused by the direct interaction between the host and virus genome, partial insertion of the viral genome into the host, and certain virus-encoded transcripts or proteins. In addition, characterizing the altered function of chromatin remodelers and the detailed process of host chromatin marginalization during BmNPV infection may help to further understand this topic.

Apart from the interaction between host chromatin, we also detected the DNA interaction of the virus–host and virus–virus (Supplemental Fig. S7A,B; Supplemental Tables S6, S7). These categories of DNA interactions have been reported in other viruses as an approach to use host machinery for their own replication and gene expression (Moquin et al. 2018; Moreau et al. 2018). Because the replication, transcription, and assembly of baculoviruses occur in the host nuclei, which require both viral and host factors (Blissard and Theilmann 2018), the DNA connection between baculovirus and host may conduce to viral assembly and egress. Homologous regions (hrs) are conserved and interspersed repetitive sequences in the baculovirus genome (Cochran and Faulkner 1983). They have been reported in earlier studies with pivotal roles in viral DNA replication, progeny production, and transcriptional enhancement (Guarino and Summers 1986; Hu et al. 2022), in which the *cis*-interaction of viral genome is indispensable. Therefore, deeper investigations on the roles of these categories of DNA interactions in baculovirus infection will shed light on virus–host interaction and viral strategies to orchestrate their life cycles by making changes to both host and viral genetic regulatory network.

## Methods

### Cell culture, virus strain, and infection

BmN cells were cultured at 27°C in SF900 II SFM (Gibco) supplemented with 3% fetal bovine serum (FBS; Gibco). The T3 strain of BmNPV was maintained in our laboratory and used as the wild-type (WT) virus. For infection, BmN cells were inoculated with BmNPV (multiplicity of infection [MOI] = 10) for 1 h at 27°C; then, the supernatant was replaced with fresh Sf-900 II SFM medium, and this time point was defined as 0 h p.i.

### Plasmids and transfection

The plasmid used for transient expression of HA-tagged BmBRD4 (gene ID 101735474) (Supplemental Fig. S3A), the plasmids for enhancer activity analysis (Supplemental Fig. S9B), the plasmid serving as the internal reference of the luciferase assays (Supplemental Fig. S9A), and the plasmid PB-luc-Zeo (Supplemental Fig. S9C) were generated from pNL1.1 (Promega E1001), pGL4.10 (Promega E6651), and pIZ/V5-His, which was preserved in our laboratory. All insertion fragments of the plasmids were confirmed by sequencing in both directions, and sequences of the primers used for plasmid construction are listed in Supplemental Table S1. Plasmid transfection was conducted using Lipo8000 (Beyotime C0533) as described previously (Zhao et al. 2022). The details are available in the Supplemental Methods.

### Preparation and sequencing of BmBRD4 ChIP-seq libraries

BmN cells ($5 \times 10^7$) were transfected with pIZ-BmBRD4-HA and treated with DMSO or 0.5 μM of JQ1 at 48 h post transcription. After 48 h of treatment, cells were cross-linked and lysed. The sheared chromatin was immunoprecipitated by anti-HA antibody (Abcam 9110) to generate the library for sequencing. The details are available in the Supplemental Methods.

### Data obtained from public databases

The ATAC-seq and ChIP-seq data except for BmBRD4 ChIP-seq were obtained from the NCBI BioProject database (https://www.ncbi.nlm.nih.gov/bioproject/) under accession numbers PRJNA549316, PRJNA628845, PRJDB1761, PRJDB2874, and PRJNA450142. The RNA-seq data of silkworm tissues were obtained from the NCBI Sequence Read Archive (SRA; https://www.ncbi.nlm.nih.gov/sra/) under accession numbers DRR030436, DRR030437, DRR030438, DRR077427, DRR290110, SRR18045785, SRR25499146, and SRR25700523.

### Processing and visualization of ATAC-seq and ChIP-seq data

ATAC-seq and ChIP-seq data were mapped to the reference *B. mori* genome (SilkBase November 2016) (Kawamoto et al. 2019) using Bowtie 2 (version 2.4.4) (Langmead and Salzberg 2012). MACS2 (version 2.2.7.1) was adopted for peak calling (Zhang et al. 2008), and deepTools (version 3.5.1) (Ramírez et al. 2014) was

used for visualization of the sequencing data. The details are available in the Supplemental Methods.

### Generation of in situ Hi-C libraries and analysis of sequencing data

The Hi-C libraries were constructed as described in previous studies (Rao et al. 2014). The DNA in the nuclei was digested by the restriction enzyme MboI, and the cohesive ends were marked with biotin-14-dCTP. The marked DNA fragments were pulled down to generate the library for sequencing.

For Hi-C analysis, the filtered data were mapped to *B. mori* genome (SilkBase) using Bowtie 2. ICE was used to generate the interaction matrix (Imakaev et al. 2012). The valid pairs were binned into 10 kb to generate contact matrices. The reproducibility between the two replicates was represented by the Pearson correlation coefficient and the stratum-adjusted correlation (Yang et al. 2017). Fit-Hi-C (version 2.0.8) was used to determine the significant interactions with the cut off of FDR 0.01 (Ay et al. 2014). The details are available in the Supplemental Methods.

### Construction of enhancer maps

The ABC model was adopted to predict enhancer–gene connections, based on measurements of chromatin accessibility (ATAC-seq), histone modifications (H3K27ac ChIP-seq), and DNA interaction frequency (Hi-C), as previously described (Fulco et al. 2019). The quantitative effect of an enhancer depends on the frequency with which it contacts a promoter multiplied by the strength of the enhancer. First, the candidate enhancer regions were defined using ATAC-seq peaks obtained by MACS2, and the promoter regions were defined as −250 bp to 250 bp of the TSS. Afterward, ATAC-seq and H3K27ac ChIP-seq reads in candidate enhancer regions were counted to quantify enhancer activity. Finally, the ABC score for each enhancer–gene pair, which means the enhancer regulatory effect to the gene, was computed by combining enhancer activity and Knight–Ruiz normalized Hi-C contact frequency between the pairs (Knight and Daniel 2013). The default ABC score threshold of 0.02 was used as the cut value, and only the enhancers within 5 Mb of each gene were considered.

### Identification of SEs

SEs were identified according to the protocol described previously (Whyte et al. 2013). Briefly, enhancers within 12.5 kb are grouped together as a cluster using BEDTools (version 2.30.0) (Quinlan and Hall 2010). Afterward, all clusters were ranked by increasing total background-subtracted ChIP-seq occupancy of H3K27ac, and the H3K27ac signal intensity was plotted. The plot revealed a clear point in the distribution of enhancers where the occupancy signal began increasing rapidly. To geometrically define this point, the data were scaled so that the *x*- and *y*-axes were from zero to one, and a point was found for which a line with a slope of one was tangent to the curve. Enhancers above this point were defined as SEs, and enhancers below this point were TEs.

### RNA sequencing and data analysis

BmN cells ($1 \times 10^6$) with indicated treatments were harvested, and total RNA of the cells was extracted to generate the library for sequencing. Three independent libraries of each treatment were analyzed. Mapped reads at the exons of each gene were counted via featureCounts, which is a part of Subread (version 2.0.1) (Liao et al. 2014). The read counts were normalized as fragments per kilobase of exon model per million mapped fragments (FPKM) using a custom R script (Supplemental Code; R Core Team 2022). Differential expression analysis of two groups was performed using R package DESeq2 (version 1.28.1) (Love et al. 2014). The details are available in the Supplemental Methods.

### GO and KEGG analysis

For functional analysis of enhancer-associated and SE-associated genes, GO annotations were obtained from R package GO.db (version 3.11.4) (https://bioconductor.org/packages/release/data/annotation/html/GO.db.html), and KEGG annotations were downloaded from the KEGG database (Kanehisa and Goto 2000). The R package clusterProfiler was applied to automate the process of biological-term classification and the enrichment analysis of gene clusters (Yu et al. 2012).

### Apoptosis detection and cell viability assay of BmN cells

Apoptosis state was determined using the Annexin V-FITC/PI apoptosis detection kit (Vazyme A211) according to the manufacturer's instructions. Cell viability was determined using the cell counting kit-8 (Beyotime C0038) according to the protocol provided by the manufacturers. The details are available in the Supplemental Methods.

### Gene silencing

To silence the genes of interest, we used RNAi by generating dsRNAs synthesized in vitro using the T7 RNAi transcription kit (Vazyme TR102) according to the manufacturer's instructions. Plasmid transfection was conducted using LipoRNAi (Beyotime C0535) as described previously (Zhao et al. 2022). The details are available in the Supplemental Methods.

### qRT-PCR analysis

BmN cells ($1 \times 10^6$) were treated as indicated. Total RNA of the cells was extracted, and the first-strand cDNAs were synthesized. Reactions were run on a real-time PCR thermal cycler (Bio-Rad). *Bmrpl32* (gene ID 778453) was used for normalizing the data. Three technical replicates for each of the three biological replicates per treatment were analyzed using the $2^{-\Delta\Delta Ct}$ method to calculate the relative expression levels of selected genes. The details are available in the Supplemental Methods.

### Analysis of viral growth curve and genome copies

Viral growth curve and genome copies analysis was conducted as described previously (Zhao et al. 2022). The titers of BV were determined by $TCID_{50}$ end point dilution assay in BmN cells (Kärber 1931). Three biological replicates were analyzed for each group. Viral gDNA copies were determined by quantification of the viral gene *gp41* (gene ID 1488698) by qPCR. *Bmrpl27* (gene ID 692703) served as an internal normalization control, and the 0-h sample was used as input to normalize the data. Three technical replicates for each of the three biological replicates were analyzed for each group. The details are available in the Supplemental Methods.

### Luciferase assays

Dual luciferase reporter assay was performed using Nano-Glo dual-luciferase reporter assay system (Promega N1610) according to the manufacturer's instructions. The luminescent signal was measured by a microplate reader (Bio Tek), and the relative light units were normalized using the firefly luminescence to indicate the promoter activity. Two technical replicates for each of the three biological

replicates per treatment were analyzed. The details are available in the Supplemental Methods.

### Immunofluorescence

BmN cells transfected with pIZ-BmBRD4-HA on the coverslips were fixed, permeabilized, and blocked. Then, the cells were incubated with anti-HA anti-body (Abcam 9110), secondary FITC-conjugated antibody (Sangon D110068), and DAPI (Beyotime C1005) successively for confocal scanning. The details are available in the Supplemental Methods.

### Western blot

Western blot was conducted as described previously (Zhao et al. 2022). The details are available in the Supplemental Methods.

## Data access

All raw sequencing data generated in this study have been submitted to the NCBI BioProject database (https://www.ncbi.nlm.nih.gov/bioproject/) under accession numbers PRJNA949399, PRJNA949409, and PRJNA1005022.

## Competing interest statement

The authors declare no competing interests.

## Acknowledgments

This work was supported by the National Natural Science Foundation of China (32172792/31972619) and the Natural Science Foundation of Zhejiang Province (Z20C170008).

*Author contributions:* S.D.Z. and X.F.W. conceived the investigation; S.D.Z. conducted most of the biochemical experiments and bioinformatic analysis; Y.D.L. performed the apoptosis detection and cell viability assay; G.P.C. and X.Y.W. constructed some of the vectors for luciferase reporter assays with the help of N.C.; N.C. performed western blot assay; S.D.Z. interpreted results and wrote the manuscript; and X.F.W. reviewed and edited the manuscript.

## References

Andersson R, Sandelin A. 2020. Determinants of enhancer and promoter activities of regulatory elements. *Nat Rev Genet* **21:** 71–87. doi:10.1038/s41576-019-0173-8

Andersson R, Gebhard C, Miguel-Escalada I, Hoof I, Bornholdt J, Boyd M, Chen Y, Zhao X, Schmidl C, Suzuki T, et al. 2014. An atlas of active enhancers across human cell types and tissues. *Nature* **507:** 455–461. doi:10.1038/nature12787

Ay F, Bailey TL, Noble WS. 2014. Statistical confidence estimation for Hi-C data reveals regulatory chromatin contacts. *Genome Res* **24:** 999–1011. doi:10.1101/gr.160374.113

Beagrie RA, Pombo A. 2016. Gene activation by metazoan enhancers: diverse mechanisms stimulate distinct steps of transcription. *Bioessays* **38:** 881–893. doi:10.1002/bies.201600032

Blissard GW, Theilmann DA. 2018. Baculovirus entry and egress from insect cells. *Annu Rev Virol* **5:** 113–139. doi:10.1146/annurev-virology-092917-043356

Braga DL, Mousovich-Neto F, Tonon-da-Silva G, Salgueiro WG, Mori MA. 2020. Epigenetic changes during ageing and their underlying mechanisms. *Biogerontology* **21:** 423–443. doi:10.1007/s10522-020-09874-y

Cao C, Hong P, Huang X, Lin D, Cao G, Wang L, Feng B, Wu P, Shen H, Xu Q, et al. 2020. HPV-CCDC106 integration alters local chromosome architecture and hijacks an enhancer by three-dimensional genome structure remodeling in cervical cancer. *J Genet Genomics* **47:** 437–450. doi:10.1016/j.jgg.2020.05.006

Çevik RE, Cesarec M, Da Silva Filipe A, Licastro D, McLauchlan J, Marcello A. 2017. Hepatitis C virus NS5A targets nucleosome assembly protein NAP1L1 to control the innate cellular response. *J Virol* **91:** e00880-17. doi:10.1128/JVI.00880-17

Chang J, Wang R, Yu K, Zhang T, Chen X, Liu Y, Shi R, Wang X, Xia Q, Ma S. 2020a. Genome-wide CRISPR screening reveals genes essential for cell viability and resistance to abiotic and biotic stresses in *Bombyx mori*. *Genome Res* **30:** 757–767. doi:10.1101/gr.249045.119

Chang YN, Zhu C, Jiang J, Zhang H, Zhu JK, Duan CG. 2020b. Epigenetic regulation in plant abiotic stress responses. *J Integr Plant Biol* **62:** 563–580. doi:10.1111/jipb.12901

Chen K, Rajewsky N. 2007. The evolution of gene regulation by transcription factors and microRNAs. *Nat Rev Genet* **8:** 93–103. doi:10.1038/nrg1990

Chen J, Lu Z, Gong W, Xiao X, Feng X, Li W, Shan S, Xu D, Zhou Z. 2022. Epstein-Barr virus protein BKRF4 restricts nucleosome assembly to suppress host antiviral responses. *Proc Natl Acad Sci* **119:** e2203782119. doi:10.1073/pnas.2203782119

Cheng D, Cheng T, Yang X, Zhang Q, Fu J, Feng T, Gong J, Xia Q. 2018. The genome-wide transcriptional regulatory landscape of ecdysone in the silkworm. *Epigenetics Chromatin* **11:** 48. doi:10.1186/s13072-018-0216-y

Cochran MA, Faulkner P. 1983. Location of homologous DNA sequences interspersed at five regions in the baculovirus AcMNPV genome. *J Virol* **45:** 961–970. doi:10.1128/jvi.45.3.961-970.1983

Daman AW, Josefowicz SZ. 2021. Epigenetic and transcriptional control of interferon-β. *J Exp Med* **218:** e20210039. doi:10.1084/jem.20210039

Dawson MA, Kouzarides T. 2012. Cancer epigenetics: from mechanism to therapy. *Cell* **150:** 12–27. doi:10.1016/j.cell.2012.06.013

Dekker J, Rippe K, Dekker M, Kleckner N. 2002. Capturing chromosome conformation. *Science* **295:** 1306–1311. doi:10.1126/science.1067799

Dominguez R, Holmes KC. 2011. Actin structure and function. *Annu Rev Biophys* **40:** 169–186. doi:10.1146/annurev-biophys-042910-155359

Dostie J, Richmond TA, Arnaout RA, Selzer RR, Lee WL, Honan TA, Rubio ED, Krumm A, Lamb J, Nusbaum C, et al. 2006. Chromosome conformation capture carbon copy (5C): a massively parallel solution for mapping interactions between genomic elements. *Genome Res* **16:** 1299–1309. doi:10.1101/gr.5571506

The ENCODE Project Consortium. 2012. An integrated encyclopedia of DNA elements in the human genome. *Nature* **489:** 57–74. doi:10.1038/nature11247

Field A, Adelman K. 2020. Evaluating enhancer function and transcription. *Annu Rev Biochem* **89:** 213–234. doi:10.1146/annurev-biochem-011420-095916

Fulco CP, Nasser J, Jones TR, Munson G, Bergman DT, Subramanian V, Grossman SR, Anyoha R, Doughty BR, Patwardhan TA, et al. 2019. Activity-by-contact model of enhancer-promoter regulation from thousands of CRISPR perturbations. *Nat Genet* **51:** 1664–1669. doi:10.1038/s41588-019-0538-0

Furlong EEM, Levine M. 2018. Developmental enhancers and chromosome topology. *Science* **361:** 1341–1345. doi:10.1126/science.aau0320

Gomi S, Majima K, Maeda S. 1999. Sequence analysis of the genome of *Bombyx mori* nucleopolyhedrovirus. *J Gen Virol* **80(Pt 5):** 1323–1337. doi:10.1099/0022-1317-80-5-1323

Groves IJ, Drane ELA, Michalski M, Monahan JM, Scarpini CG, Smith SP, Bussotti G, Várnai C, Schoenfelder S, Fraser P, et al. 2021. Short- and long-range cis interactions between integrated HPV genomes and cellular chromatin dysregulate host gene expression in early cervical carcinogenesis. *PLoS Pathog* **17:** e1009875. doi:10.1371/journal.ppat.1009875

Guarino LA, Summers MD. 1986. Interspersed homologous DNA of *Autographa californica* nuclear polyhedrosis virus enhances delayed-early gene expression. *J Virol* **60:** 215–223. doi:10.1128/jvi.60.1.215-223.1986

Haberle V, Stark A. 2018. Eukaryotic core promoters and the functional basis of transcription initiation. *Nat Rev Mol Cell Biol* **19:** 621–637. doi:10.1038/s41580-018-0028-8

Hamajima R, Iwamoto A, Tomizaki M, Suganuma I, Kitaguchi K, Kobayashi M, Yamada H, Ikeda M. 2016. Functional analysis of inhibitor of apoptosis 1 of the silkworm *Bombyx mori*. *Insect Biochem Mol Biol* **79:** 97–107. doi:10.1016/j.ibmb.2016.10.012

Heintzman ND, Hon GC, Hawkins RD, Kheradpour P, Stark A, Harp LF, Ye Z, Lee LK, Stuart RK, Ching CW, et al. 2009. Histone modifications at human enhancers reflect global cell-type-specific gene expression. *Nature* **459:** 108–112. doi:10.1038/nature07829

Heinz S, Texari L, Hayes MGB, Urbanowski M, Chang MW, Givarkes N, Rialdi A, White KM, Albrecht RA, Pache L, et al. 2018. Transcription elongation can affect genome 3D structure. *Cell* **174:** 1522–1536.e22. doi:10.1016/j.cell.2018.07.047

Hnisz D, Abraham BJ, Lee TI, Lau A, Saint-André V, Sigova AA, Hoke HA, Young RA. 2013. Super-enhancers in the control of cell identity and disease. *Cell* **155:** 934–947. doi:10.1016/j.cell.2013.09.053

Hnisz D, Shrinivas K, Young RA, Chakraborty AK, Sharp PA. 2017. A phase separation model for transcriptional control. *Cell* **169:** 13–23. doi:10.1016/j.cell.2017.02.007

Hu H, Pan K, Shang Y, Guo Y, Xiao H, Deng F, Wang M, Hu Z. 2022. Multiloci manipulation of baculovirus genome reveals the pivotal role of homologous regions in viral DNA replication, progeny production, and enhancing transcription. *ACS Synth Biol* **11:** 144–153. doi:10.1021/acssynbio.1c00303

Imakaev M, Fudenberg G, McCord RP, Naumova N, Goloborodko A, Lajoie BR, Dekker J, Mirny LA. 2012. Iterative correction of Hi-C data reveals hallmarks of chromosome organization. *Nat Methods* **9:** 999–1003. doi:10.1038/nmeth.2148

Jia R, Chai P, Zhang H, Fan X. 2017. Novel insights into chromosomal conformations in cancer. *Mol Cancer* **16:** 173. doi:10.1186/s12943-017-0741-5

Jiang L, Xia Q. 2014. The progress and future of enhancing antiviral capacity by transgenic technology in the silkworm *Bombyx mori*. *Insect Biochem Mol Biol* **48:** 1–7. doi:10.1016/j.ibmb.2014.02.003

Jiang S, Zhou H, Liang J, Gerdt C, Wang C, Ke L, Schmidt SCS, Narita Y, Ma Y, Wang S, et al. 2017. The Epstein-Barr virus regulome in lymphoblastoid cells. *Cell Host Microbe* **22:** 561–573.e4. doi:10.1016/j.chom.2017.09.001

Junge W, Nelson N. 2015. ATP synthase. *Annu Rev Biochem* **84:** 631–657. doi:10.1146/annurev-biochem-060614-034124

Kanehisa M, Goto S. 2000. KEGG: Kyoto Encyclopedia of Genes and Genomes. *Nucleic Acids Res* **28:** 27–30. doi:10.1093/nar/28.1.27

Kärber G. 1931. Beitrag zur kollektiven Behandlung pharmakologischer Reihenversuche. *Naunyn-Schmiedebergs Archiv für experimentelle Pathologie und Pharmakologie* **162:** 480–483. doi:10.1007/BF01863914

Kawamoto M, Jouraku A, Toyoda A, Yokoi K, Minakuchi Y, Katsuma S, Fujiyama A, Kiuchi T, Yamamoto K, Shimada T. 2019. High-quality genome assembly of the silkworm, *Bombyx mori*. *Insect Biochem Mol Biol* **107:** 53–62. doi:10.1016/j.ibmb.2019.02.002

Kim KD, Tanizawa H, De Leo A, Vladimirova O, Kossenkov A, Lu F, Showe LC, Noma KI, Lieberman PM. 2020. Epigenetic specifications of host chromosome docking sites for latent Epstein-Barr virus. *Nat Commun* **11:** 877. doi:10.1038/s41467-019-14152-8

Knight PA, Daniel R. 2013. A fast algorithm for matrix balancing. *IMA J Numer Anal* **33:** 1029–1047. doi:10.1093/imanum/drs019

Kondo A, Maeda S. 1991. Host range expansion by recombination of the baculoviruses *Bombyx mori* nuclear polyhedrosis virus and *Autographa californica* nuclear polyhedrosis virus. *J Virol* **65:** 3625–3632. doi:10.1128/jvi.65.7.3625-3632.1991

Kong X, Wei G, Chen N, Zhao S, Shen Y, Zhang J, Li Y, Zeng X, Wu X. 2020. Dynamic chromatin accessibility profiling reveals changes in host genome organization in response to baculovirus infection. *PLoS Pathog* **16:** e1008633. doi:10.1371/journal.ppat.1008633

Laakkonen JP, Kaikkonen MU, Ronkainen PH, Ihalainen TO, Niskanen EA, Häkkinen M, Salminen M, Kulomaa MS, Ylä-Herttuala S, Airenne KJ, et al. 2008. Baculovirus-mediated immediate-early gene expression and nuclear reorganization in human cells. *Cell Microbiol* **10:** 667–681. doi:10.1111/j.1462-5822.2007.01074.x

Lacey LA, Grzywacz D, Shapiro-Ilan DI, Frutos R, Brownbridge M, Goettel MS. 2015. Insect pathogens as biological control agents: back to the future. *J Invertebr Pathol* **132:** 1–41. doi:10.1016/j.jip.2015.07.009

Langmead B, Salzberg SL. 2012. Fast gapped-read alignment with Bowtie 2. *Nat Methods* **9:** 357–359. doi:10.1038/nmeth.1923

Li C, Fan Y, Li G, Xu X, Duan J, Li R, Kang X, Ma X, Chen X, Ke Y, et al. 2018. DNA methylation reprogramming of functional elements during mammalian embryonic development. *Cell Discov* **4:** 41. doi:10.1038/s41421-018-0039-9

Li F, An Z, Zhang Z. 2019. The dynamic 3D genome in gametogenesis and early embryonic development. *Cells* **8:** 788. doi:10.3390/cells8080788

Liang W, Wang S, Wang H, Li X, Meng Q, Zhao Y, Zheng C. 2022. When 3D genome technology meets viral infection, including SARS-CoV-2. *J Med Virol* **94:** 5627–5639. doi:10.1002/jmv.28040

Liao Y, Smyth GK, Shi W. 2014. featureCounts: an efficient general purpose program for assigning sequence reads to genomic features. *Bioinformatics* **30:** 923–930.

Lieberman PM. 2008. Chromatin organization and virus gene expression. *J Cell Physiol* **216:** 295–302. doi:10.1002/jcp.21421

Lieberman-Aiden E, van Berkum NL, Williams L, Imakaev M, Ragoczy T, Telling A, Amit I, Lajoie BR, Sabo PJ, Dorschner MO, et al. 2009. Comprehensive mapping of long-range interactions reveals folding principles of the human genome. *Science* **326:** 289–293. doi:10.1126/science.1181369

Long HK, Prescott SL, Wysocka J. 2016. Ever-changing landscapes: transcriptional enhancers in development and evolution. *Cell* **167:** 1170–1187. doi:10.1016/j.cell.2016.09.018

Love MI, Huber W, Anders S. 2014. Moderated estimation of fold change and dispersion for RNA-seq data with DESeq2. *Genome Biol* **15:** 550. doi:10.1186/s13059-014-0550-8

Lovén J, Hoke HA, Lin CY, Lau A, Orlando DA, Vakoc CR, Bradner JE, Lee TI, Young RA. 2013. Selective inhibition of tumor oncogenes by disruption of super-enhancers. *Cell* **153:** 320–334. doi:10.1016/j.cell.2013.03.036

Millán-Zambrano G, Burton A, Bannister AJ, Schneider R. 2022. Histone post-translational modifications: cause and consequence of genome function. *Nat Rev Genet* **23:** 563–580. doi:10.1038/s41576-022-00468-7

Mishra V. 2020. A comprehensive guide to the commercial baculovirus expression vector systems for recombinant protein production. *Protein Pept Lett* **27:** 529–537. doi:10.2174/0929866526666191112152646

Moquin SA, Thomas S, Whalen S, Warburton A, Fernandez SG, McBride AA, Pollard KS, Miranda JL. 2018. The Epstein-Barr virus episome maneuvers between nuclear chromatin compartments during reactivation. *J Virol* **92:** e01413-17. doi:10.1128/JVI.01413-17

Moreau P, Cournac A, Palumbo GA, Marbouty M, Mortaza S, Thierry A, Cairo S, Lavigne M, Koszul R, Neuveut C. 2018. Tridimensional infiltration of DNA viruses into the host genome shows preferential contact with active chromatin. *Nat Commun* **9:** 4268. doi:10.1038/s41467-018-06739-4

Morillon A, Karabetsou N, Nair A, Mellor J. 2005. Dynamic lysine methylation on histone H3 defines the regulatory phase of gene transcription. *Mol Cell* **18:** 723–734. doi:10.1016/j.molcel.2005.05.009

Nagamine T, Kawasaki Y, Abe A, Matsumoto S. 2008. Nuclear marginalization of host cell chromatin associated with expansion of two discrete virus-induced subnuclear compartments during baculovirus infection. *J Virol* **82:** 6409–6418. doi:10.1128/JVI.00490-08

Padeken J, Methot SP, Gasser SM. 2022. Establishment of H3K9-methylated heterochromatin and its functions in tissue differentiation and maintenance. *Nat Rev Mol Cell Biol* **23:** 623–640. doi:10.1038/s41580-022-00483-w

Palmateer CM, Moseley SC, Ray S, Brovero SG, Arbeitman MN. 2021. Analysis of cell-type-specific chromatin modifications and gene expression in *Drosophila* neurons that direct reproductive behavior. *PLoS Genet* **17:** e1009240. doi:10.1371/journal.pgen.1009240

Quinlan AR, Hall IM. 2010. BEDTools: a flexible suite of utilities for comparing genomic features. *Bioinformatics* **26:** 841–842.

Ramírez F, Dündar F, Diehl S, Grüning BA, Manke T. 2014. deepTools: a flexible platform for exploring deep-sequencing data. *Nucleic Acids Res* **42:** W187–W191. doi:10.1093/nar/gku365

Rao SS, Huntley MH, Durand NC, Stamenova EK, Bochkov ID, Robinson JT, Sanborn AL, Machol I, Omer AD, Lander ES, et al. 2014. A 3D map of the human genome at kilobase resolution reveals principles of chromatin looping. *Cell* **159:** 1665–1680. doi:10.1016/j.cell.2014.11.021

R Core Team. 2022. *R: a language and environment for statistical computing*. R Foundation for Statistical Computing, Vienna. https://www.R-project.org/.

Richter K, Haslbeck M, Buchner J. 2010. The heat shock response: life on the verge of death. *Mol Cell* **40:** 253–266. doi:10.1016/j.molcel.2010.10.006

Roadmap Epigenomics Consortium, Kundaje A, Meuleman W, Ernst J, Bilenky M, Yen A, Heravi-Moussavi A, Kheradpour P, Zhang Z, Wang J, Ziller MJ, et al. 2015. Integrative analysis of 111 reference human epigenomes. *Nature* **518:** 317–330. doi:10.1038/nature14248

Rohrmann GF. 2013. *Baculovirus molecular biology*. National Center for Biotechnology Information, Bethesda, MD.

Sabari BR, Dall'Agnese A, Boija A, Klein IA, Coffey EL, Shrinivas K, Abraham BJ, Hannett NM, Zamudio AV, Manteiga JC, et al. 2018. Coactivator condensation at super-enhancers links phase separation and gene control. *Science* **361:** ear3958. doi:10.1126/science.aar3958

Santos-Rosa H, Schneider R, Bannister AJ, Sherriff J, Bernstein BE, Emre NC, Schreiber SL, Mellor J, Kouzarides T. 2002. Active genes are tri-methylated at K4 of histone H3. *Nature* **419:** 407–411. doi:10.1038/nature01080

Schoenfelder S, Fraser P. 2019. Long-range enhancer-promoter contacts in gene expression control. *Nat Rev Genet* **20:** 437–455. doi:10.1038/s41576-019-0128-0

Shibata Y, Sheffield NC, Fedrigo O, Babbitt CC, Wortham M, Tewari AK, London D, Song L, Lee BK, Iyer VR, et al. 2012. Extensive evolutionary changes in regulatory element activity during human origins are associated with altered gene expression and positive selection. *PLoS Genet* **8:** e1002789. doi:10.1371/journal.pgen.1002789

Shlyueva D, Stampfel G, Stark A. 2014. Transcriptional enhancers: from properties to genome-wide predictions. *Nat Rev Genet* **15:** 272–286. doi:10.1038/nrg3682

Shoji K, Kokusho R, Kawamoto M, Suzuki Y, Katsuma S. 2021. H3k4me3 histone modification in baculovirus-infected silkworm cells. *Virus Genes* **57:** 459–463. doi:10.1007/s11262-021-01858-5

Simonis M, Klous P, Splinter E, Moshkin Y, Willemsen R, de Wit E, van Steensel B, de Laat W. 2006. Nuclear organization of active and inactive chromatin domains uncovered by chromosome conformation capture-on-chip (4C). *Nat Genet* **38:** 1348–1354. doi:10.1038/ng1896

Smale ST, Kadonaga JT. 2003. The RNA polymerase II core promoter. *Annu Rev Biochem* **72:** 449–479. doi:10.1146/annurev.biochem.72.121801.161520

Spitz F, Furlong EE. 2012. Transcription factors: from enhancer binding to developmental control. *Nat Rev Genet* **13:** 613–626. doi:10.1038/nrg3207

Sun L, Yu R, Dang W. 2018. Chromatin architectural changes during cellular senescence and aging. *Genes (Basel)* **9:** 211. doi:10.3390/genes9040211

Tserel L, Kolde R, Rebane A, Kisand K, Org T, Peterson H, Vilo J, Peterson P. 2010. Genome-wide promoter analysis of histone modifications in human monocyte-derived antigen presenting cells. *BMC Genomics* **11:** 642. doi:10.1186/1471-2164-11-642

Vidaurre V, Chen X. 2021. Epigenetic regulation of *Drosophila* germline stem cell maintenance and differentiation. *Dev Biol* **473:** 105–118. doi:10.1016/j.ydbio.2021.02.003

Visel A, Rubin EM, Pennacchio LA. 2009. Genomic views of distant-acting enhancers. *Nature* **461:** 199–205. doi:10.1038/nature08451

Wang HC, Wang HC, Ko TP, Lee YM, Leu JH, Ho CH, Huang WP, Lo CF, Wang AH. 2008. White spot syndrome virus protein ICP11: a histone-binding DNA mimic that disrupts nucleosome assembly. *Proc Natl Acad Sci* **105:** 20758–20763. doi:10.1073/pnas.0811233106

Wang X, Cairns MJ, Yan J. 2019. Super-enhancers in transcriptional regulation and genome organization. *Nucleic Acids Res* **47:** 11481–11496.

Wang L, Laing J, Yan B, Zhou H, Ke L, Wang C, Narita Y, Zhang Z, Olson MR, Afzali B, et al. 2020. Epstein-Barr virus episome physically interacts with active regions of the host genome in lymphoblastoid cells. *J Virol* **94:** e01390-20. doi:10.1128/JVI.01390-20

Weitzman MD, Fradet-Turcotte A. 2018. Virus DNA replication and the host DNA damage response. *Annu Rev Virol* **5:** 141–164. doi:10.1146/annurev-virology-092917-043534

Whalen S, Truty RM, Pollard KS. 2016. Enhancer–promoter interactions are encoded by complex genomic signatures on looping chromatin. *Nat Genet* **48:** 488–496. doi:10.1038/ng.3539

Whyte WA, Orlando DA, Hnisz D, Abraham BJ, Lin CY, Kagey MH, Rahl PB, Lee TI, Young RA. 2013. Master transcription factors and mediator establish super-enhancers at key cell identity genes. *Cell* **153:** 307–319. doi:10.1016/j.cell.2013.03.035

Xiao S, Huang Q, Ren H, Yang M. 2021. The mechanism and function of super enhancer RNA. *Genesis* **59:** e23422. doi:10.1002/dvg.23422

Yang T, Zhang F, Yardımcı GG, Song F, Hardison RC, Noble WS, Yue F, Li Q. 2017. HiCRep: assessing the reproducibility of Hi-C data using a stratum-adjusted correlation coefficient. *Genome Res* **27:** 1939–1949. doi:10.1101/gr.220640.117

Yang B, Li B, Jia L, Jiang Y, Wang X, Jiang S, Du S, Ji X, Yang P. 2020. 3D landscape of hepatitis B virus interactions with human chromatins. *Cell Discov* **6:** 95. doi:10.1038/s41421-020-00218-1

Yu G, Wang LG, Han Y, He QY. 2012. clusterProfiler: an R package for comparing biological themes among gene clusters. *Omics* **16:** 284–287. doi:10.1089/omi.2011.0118

Zhang Q, Cao X. 2019. Epigenetic regulation of the innate immune response to infection. *Nat Rev Immunol* **19:** 417–432. doi:10.1038/s41577-019-0151-6

Zhang Y, Liu T, Meyer CA, Eeckhoute J, Johnson DS, Bernstein BE, Nusbaum C, Myers RM, Brown M, Li W, et al. 2008. Model-based Analysis of ChIP-seq (MACS). *Genome Biol* **9:** R137. doi:10.1186/gb-2008-9-9-r137

Zhao Z, Tavoosidana G, Sjölinder M, Göndör A, Mariano P, Wang S, Kanduri C, Lezcano M, Sandhu KS, Singh U, et al. 2006. Circular chromosome conformation capture (4C) uncovers extensive networks of epigenetically regulated intra- and interchromosomal interactions. *Nat Genet* **38:** 1341–1347. doi:10.1038/ng1891

Zhao S, Chen G, Kong X, Chen N, Wu X. 2022. BmNPV p35 reduces the accumulation of virus-derived siRNAs and hinders the function of siRNAs to facilitate viral infection. *Front Immunol* **13:** 845268. doi:10.3389/fimmu.2022.845268

*Received March 28, 2023; accepted in revised form October 14, 2023.*